EQUIVALENT CIRCUIT MODELING OF TMS PLASMA POLYMER COATING SYSTEMS ON COLD-ROLLED STEEL

A Thesis presented to the Faculty of the Graduate School
University of Missouri-Columbia

In Partial Fulfillment
Of the Requirements for the Degree

Master of Science

---

by
KEVIN YOUNG

Dr. Hirotsugu K. Yasuda, Thesis Supervisor

DECEMBER, 2004

The undersigned, appointed by the Dean of the Graduate School,
have examined the thesis entitled

EQUIVALENT CIRCUIT MODELING OF TMS PLASMA
POLYMER COATING SYSTEMS ON COLD-ROLLED STEEL

Presented by Kevin Young

A candidate for the degree of Master of Science

And hereby certify that in their opinion is worthy of acceptance.

Dr. Hitotsugu K. Yasuda

Dr. Qingsong Yu

Dr. James E. Bryan

ACKNOWLEDGEMENTS

I would like to thank Dr. Hirotsugu K. Yasuda for everything he has done for me as a graduate and undergraduate student. He has given me a plethora of good advice. Although not always taken advantage of in college, his wisdom and guidance will benefit me throughout my career.

I would also like to show appreciation to Dr. Qingsong Yu who not only took time to help me learn when I started in research, but since his return to the university has made himself available to assist me as I completed my requirements from a distant location. I could not have completed my undergraduate research project without the help of Dr. Christopher Weikart who also influenced me to continue for an advanced degree. Others from the research group I would like to thank are Dr. Reddy and Dr. Chen who helped me in the beginning, and Mary Gilliam who was an excellent student allowing me to pass down the knowledge I had gained to continue plasma research at the University of Missouri-Columbia.

I could not have done this without the support of my family. My parents, Earl and Rosemarie, were always there for me, emotionally and financially. Encouragement from my brother came from his words and actions as he also earned his Masters Degree this year. Congratulations, Tim.

Most importantly I would like to thank my fiancée, Erin (wife after November 6). Without her I would have never completed my thesis. Discouragement and frustration were always overcome by her motivation. I needed every loving push she gave me.

EQUIVALENT CIRCUIT MODELING OF TMS PLASMA

POLYMER COATING SYSTEMS ON COLD-ROLLED STEEL

Kevin Young

Dr. Hirotsugu K. Yasuda Thesis Supervisor

ABSTRACT

Electrochemical impedance spectroscopy (EIS) during an accelerated corrosion (GM scab) test was used to differentiate between good and poor coating systems on cold-rolled steel (CRS). The best coating was determined to be a cathodic E-coat/trimethylsilane (TMS) plasma polymer/oxide-free steel surface having an impedance modulus at low frequency of 10^9 ohms throughout the entire corrosion test. A spray paint primer and surface oxides both contributed to a degradation of corrosion protection evident from a significant drop in impedance (10^6 Ω).

With samples of known corrosion resistance, equivalent circuits were used to relate circuit elements to individual chemical processes taking place and identify the major factors contributing to failure of the coating. Two models (with and without plasma polymer film) were proposed and a good correlation to the EIS data was shown by a good visual plot fit and low chi squared values ($<10^{-3}$).

It was determined that the performance of the plasma polymer and conditions at the PP/steel interface are the major factors influencing the coating performance. The good coating system maintained a low double layer capacitance (10^{-9} F) and high charge transfer resistance (10^9 Ω) relating to good adhesion at the coating/metal interface. The other samples, which exhibited poor adhesion, had a much higher capacitance (10^{-6} F) meaning water pool formation has created a water/metal interface. This in turn allows salt penetration for a higher corrosion rate showing up in the lower resistance (10^6 Ω).

TABLE OF CONTENTS

LIST OF FIGURES

LIST OF TABLES

Table Page

1. INTRODUCTION

Zinc phosphating is the conventional method for preparing a steel surface for subsequent coatings. Metal phosphate complexes are formed resulting in a rough crystal surface, which provides anchoring sites for the organic coating. The enhanced adhesion is believed to be caused primarily by mechanical interlocking. There are several drawbacks to this process, however. The most significant one is the environmental concern phosphating incurs. For adequate corrosion protection, lead is an essential ingredient in the E-coat and galvanized steel is the required substrate hindering the recycling potential. Other negative features are the weaker substrate caused by corrosion during the phosphating process and the lack of heat stability from its crystalline nature.

In recent years, plasma polymerization has been investigated as a potential replacement for surface preparation of metallic material [1-4]. This process forms highly cross-linked polymer coatings onto the substrate surface without affecting the bulk material. With this environment friendly process, superior adhesion of the primer may be achieved which is vital to the corrosion resistance of the coating system.

Electrochemical Impedance Spectroscopy (EIS) is a powerful tool used to predict the performance of coating systems. It has been used extensively for researching corrosion resistance of coatings on aluminum alloys and steel substrates [5-7]. Most of the work to date has focused on the performance of the coating system as a whole. Recently, an equivalent circuit was developed to simulate the EIS data from coated aluminum samples and determine the critical components of the interface engineered system [8]. The objective of this study is to find a comparable equivalent circuit to model coated steel systems.

2. LITERATURE REVIEW

2.1 Corrosion Mechanism

Usually an electrochemical process, corrosion is defined as the destructive attack on a metal by chemical reaction with its environment. The corrosion reactions are oxidation-reduction reactions in which the elemental form of a metal is oxidized reducing its strength and conductive properties [9-12]. This is a result of a transfer of electrons from the anode areas to the cathode areas. The most common example is the rusting of iron, which costs billions of dollars each year in replacement and maintenance costs. The economic impact alone is a valid reason for understanding the corrosion processes.

Oxygen and moisture are the basic factors necessary for corrosion to occur. Both must be present simultaneously, because oxygen alone or water free of dissolved oxygen does not corrode iron to any practical extent. The oxygen diffuses into the water that brings the dissolved gas into contact with the metal surface. This reduction half-reaction is:

$$O_2 + 2\,H_2O + 4\,e^- \rightarrow 4\,OH^- \qquad E^0_{red} = +0.40\ V \qquad (1)$$

Because of the large reduction potential (+0.40 V), most common metals will form a spontaneous redox couple with this half-reaction. For iron, the corresponding half-reaction is:

$$Fe \rightarrow Fe^{2+} + 2\,e^- \qquad E^0_{red} = -0.44\ V \qquad (2)$$

The higher reduction potential for reaction 1 means the reduction of oxygen is favored over the reduction of iron. Thus, the iron will preferentially oxidize at the anode area. Combining the cathode (reaction 1) and anode (reaction 2) yields the overall reaction:

$$2\,Fe + O_2 + 2\,H_2O \rightarrow 2\,Fe(OH)_2 \qquad (3)$$

The $Fe(OH)_2$ product can be further oxidized to form $Fe(OH)_3$, which is then dehydrated to Fe_2O_3 with its familiar red color associated with rust.

Aluminum is an even more reactive metal than iron, having the anode half-reaction:

$$Al \rightarrow Al^{3+} + 3\,e^- \qquad E^0_{red} = -1.66\ V \qquad (4)$$

Aluminum does oxidize; however, the extent of corrosion is small compared to the corrosion of iron. This interesting phenomenon is due to the nature of the metal oxide product. Aluminum oxide (Al_2O_3) is very dense and forms a thin protective layer that adheres to the metal and discourages further corrosion. In contrast, iron rust (Fe_2O_3) is typically flaky and easily crumbles off to continually expose fresh metal for reaction.

It was mentioned earlier that both oxygen and water are required for corrosion to occur. For the corrosion to proceed at a significant rate, a complete electrical circuit is needed. Thus, the rate of corrosion is dependent upon the conductivity of the aqueous solution in which it is immersed. The conductivity is increased with the presence of dissolved salts. These ions in the water provide a salt bridge that accelerates the corrosion process.

2.2 Phosphate Coating

A current method of protecting steel from corrosion is coating the steel with another metal. Zinc is commonly used is this manner, producing a galvanized steel. The zinc layer acts as a barrier to keep oxygen and water away from the iron. If the zinc coating is worn or scratched, the zinc will electrochemically protect the iron from oxidizing. Zinc is a more active metal than iron shown by the reduction potentials in the following reactions:

$$Zn^{2+} + 2\,e^- \rightarrow Zn \qquad E^0_{red} = -0.76\ V \qquad (5)$$

$$Fe^{2+} + 2\,e^- \rightarrow Fe \qquad E^0_{red} = -0.44\ V \qquad (6)$$

Since the iron is preferentially reduced over the zinc, the zinc will serve as the anode and the iron as the cathode in a redox reaction. The zinc is termed a sacrificial anode because it will oxidize to provide cathodic protection.

Typically, it is difficult to achieve good adhesion between a paint coating and a fresh galvanized steel sheet. For this reason, it is customary to apply some type of intermediate layer, a pretreatment, to develop good long-term performance. Not only does the pretreatment improve the mechanical adhesion between the paint and the zinc coating, but it also improves the resistance to blistering and paint delaminating during exposure to corrosive environments.

A zinc phosphate conversion coating is the most commonly applied paint pretreatment for developing good bonding qualities between the paint and the galvanized steel [13,14]. Extremely important technology to the automotive industry, the usual zinc phosphate process involves several steps:

- Alkaline cleaning
- Water rinse
- Titanium activator rinse
- Application of the zinc phosphate solution
- Hot water rinse
- Chromic acid rinse

Degreasing is accomplished using an aqueous, alkaline cleaning solution to remove oils present on the surface of the galvanized steel. Next, there is a conditioning stage that involves the application of a titanium phosphate conditioner to prepare the galvanized surface for the development of a superior zinc phosphate coating. The titanium phosphate aids in the development of a uniform phosphate coating with small zinc

phosphate crystals by depositing sub-micron size particles which act as seeds to promote the growth of zinc phosphate crystals on the surface of the galvanized steel.

After conditioning, the zinc phosphate coating is applied by immersion in a zinc phosphate solution or by spraying zinc phosphate solution onto the substrate surface. The acidic zinc phosphate actually dissolves a small amount of the zinc coating. The acid attack of the phosphate solution produces a localized increase in the pH resulting in the precipitation and deposition of insoluble zinc phosphate crystals on the surface of the galvanized coating given by the reaction:

$$3\,Zn^{2+} + 2\,H_2PO_4^- \rightarrow Zn_3(PO)_4 + 4\,H^+ \qquad (7)$$

This crystallizing action leaves behind a continuous, relatively thick solid film of zinc phosphate on the surface of the steel sheet. The steel is then rinsed thoroughly and dried. In addition to cathodic protection, the zinc layer is passivated by a chromate layer, which improves the corrosion protection by its barrier effect.

With a zinc phosphate layer, the resultant paint adhesion is greatly improved [15]. It is said that oxygen in the phosphate film allows for some hydrogen bonding to occur between the paint and phosphate coating, however, mechanical interlocking is believed to be the primary means of adhesion [16]. This is due to the crystalline nature of the phosphate film, which provides a rough and porous surface for the subsequent paint coating to be applied.

It has been shown that zinc phosphating galvanized steel greatly improves the adhesion of paint to the metal surface, and ultimately provides excellent corrosion protection. The drawbacks to this method are the hazards that it causes. The use of a chromate rinse generates hexavalent chromium which is a known carcinogen. Other metal ions present, including lead and zinc, form a hazardous sludge in the phosphate

bath and can be released into the rinse waters. Special treatments are needed before the water can be discharged. More environmental concern comes from the inclusion of lead in the paint recipe, which is needed for the E-coat to be effective.

2.3 Plasma Polymerization

More stringent environmental regulations have led to an extensive amount of research to find an alternative to the phosphate and chromate based metal pretreatments, especially in the automotive industry. One technology with great potential is that of plasma polymerization. The focus of a significant amount of research in recent years, plasma polymerization produces ultra-thin polymer films with excellent adhesion to metal and polymer substrates along with thermal, mechanical, and chemical stability [17,18].

Many crucial material properties such as adhesion, biocompatibility, hydrophobicity, and friction are governed by the molecular state of the topmost surface. Tailoring the surface by plasma modification and polymerization is an emerging technology and revolutionized the thin film forming process. The technology is versatile and can be used for deposition of conducting/semi conducting organic films, controlling the tribology, hydrophobic/hydrophilic and biocompatible nature of the surface, modifying the transport properties of the membranes, improving adhesion, wettability, dye uptake and other technologically important surface characteristics.

Plasma polymerization is the process of forming polymeric material in glow discharge plasma. Plasma polymers deposited onto solid surfaces form ultra-thin films that are pinhole-free and made of very short segments that are highly branched, and cross-linked [19]. Plasma polymerization is considered an atomic process, which differs

dramatically from conventional polymerization which is a molecular process and contains much longer polymer segments. Minimum alteration of the chemical structure takes place when monomer molecules are linked by conventional polymerization. A plasma polymer consists of the initial monomer elements, but the structure is much more random. A graphic representation of these polymers is shown in Figure 1.

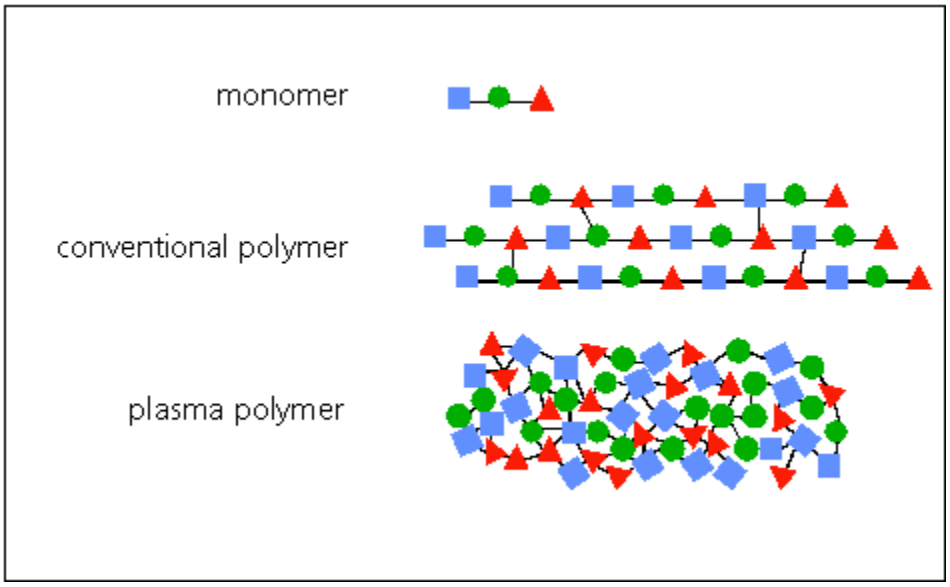

Figure 1. Illustration comparing a plasma polymer to a conventional polymer [20].

Although experimental parameters such as system pressure, monomer flow rate, and electric discharge power are important to the interaction of the plasma with the solid surface, the energy density is a better descriptor of what is taking place. The composite parameter, W/FM, where W is the discharge power, F is the monomer flow rate, and M is the molecular weight of the monomer, is frequently used to quantify the experimental conditions. More detail can be read in the literature, as Yasuda [19] has shown the significance of this parameter.

2.3.1 DC Glow Discharge

The term plasma refers to the state of partially ionized gas consisting of electrons, ions, and neutral atoms or molecules. Plasma is most commonly created by electrical discharge and is often described as low temperature plasma. Plasma polymer deposition characteristics for various power sources including DC, AF, and RF are discussed in the literature [21,22]. The scope of this study was limited to the use of a DC discharge and therefore will be the focus in this paper.

The glow discharge owes its name to the fact that plasma is luminous. The glow is produced by applying a potential difference between two electrodes in the presence of a gas. Close to the cathode, the potential drops rapidly.

The electrons have a wide distribution of energies which creates alternating luminous and dark regions. Figure 2 shows a typical schematic representation of DC glow discharge [23]. This diagram illustrates the glow in a long tube with a system pressure around 1 Torr. This, however, is not the situation in most glow discharge reactors used for plasma polymerization [24]. The reactor is larger with a shorter distance between the electrodes, and the system pressure is considerably lower (50 mTorr). Because of the short distance between the cathode and anode, the Faraday dark region is not observed and the negative glow extends to the anode, illustrated in Figure 3. As the system pressure increases, the negative glow reduces and the Faraday dark space appears near the anode.

Glow discharge plasma is known as non-equilibrium plasma, which means that the ions and neutral atoms are generally at a temperature close to room temperature, while the electrons are at extremely high temperatures. This means their kinetic energy is

very high and they move, or diffuse, at velocities many orders of magnitude more rapidly than do the heavy ions or neutral molecules.

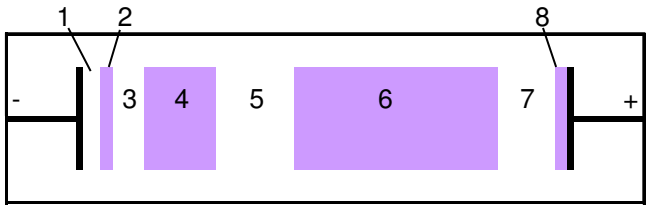

Figure 2. Illustration of the luminous regions of a glow discharge in a long tube reactor; 1) Aston dark space, 2) cathode glow, 3) cathode dark space (Crooke's), 4) negative glow, 5) Faraday dark space, 6) positive column, 7) anode dark space, 8) anode glow.

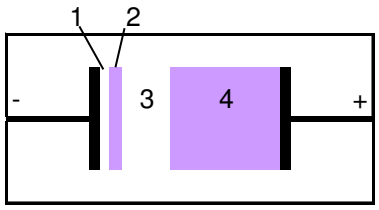

Figure 3. Illustration of the luminous regions of a glow discharge in a typical DC reactor; 1) Aston dark space, 2) cathode glow, 3) cathode dark space (Crooke's), 4) negative glow.

When the plasma is initially ignited, and a large burst of free electrons and positive ions are created from the ionization in the initial breakdown discharge, the hot electrons diffuse very rapidly away from the discharge to the positive electrode which leaves a cloud of positive ions within the bulk region of the plasma. The plasma stabilizes as more ionization takes place and diffusion out of the glow occurs until a steady state is established (all in microseconds).

The electrons quickly attain high velocity (kinetic energy) because of their low mass as they accelerate toward the anode, shown in Figure 4. They begin to collide with gas molecules, where the collisions can be either elastic or inelastic. Figure 5 illustrates the difference between these types of collisions. If the electron does not have sufficient

energy, it will undergo an elastic collision which will deplete very little of the electron's energy and not significantly influence the molecules because of their large mass compared to that of the electron. If the electron has enough kinetic energy, an inelastic collision will occur. This type of collision excites the molecules of gas or ionizes them by completely removing an electron. The excitation-relaxation processes result in the emission of photons which are responsible for the glow.

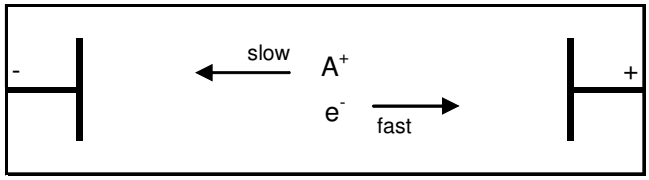

Figure 4. Illustration of ion movement within a glow discharge reactor.

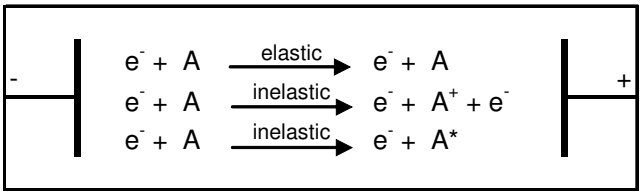

Figure 5. Illustration of elastic and inelastic collisions within a glow discharge reactor. ($A^* \rightarrow A$ + photon)

The process of ionization generates an electron that rapidly accelerates toward the anode along with the initial electron, and a positive ion that will accelerate much more slowly toward the cathode. These positive ions create additional electrons by secondary emission from the cathode. The secondary electrons are very important to maintaining a sustainable discharge.

The secondary electrons from the cathode together with the initial electrons outnumber the ions in the Aston dark space, resulting in a negative space charge. This is

a thin region adjacent to the cathode with a strong electric field that accelerates the electrons through this space away from the cathode. The electrons' kinetic energy is too low to excite the gas, so it appears dark. In the cathode glow, the electrons have become energetic enough to excite the neutral atoms they collide with. These inelastic collisions produce the glow that is observed. Occasionally the cathode glow clings to the cathode and masks the Aston dark space.

The electrons continue to accelerate in the cathode dark space, also known as Crooke's dark space. Here, the energy of the electrons is not high enough for excitation of atoms and therefore this region remains dark. The brightest intensity of the entire discharge comes from the negative glow. Electrons that have been accelerated in the cathode region to high speeds produce ionization. Slower electrons that have already had inelastic collisions produce excitations and are responsible for the negative glow. As these electrons slow down from the collisions, energy for excitation is no longer available and if present, the Faraday dark space begins.

A magnetically enhanced discharge is used to increase the electron activity within the electric field [24,25]. A magnetron can be formed by orienting bar magnets in a spoke configuration on each electrode with like poles all facing the center. Imposing an intense magnetic field forces the electrons to move in spirals instead of straight lines. This effectively increases the distance an electron travels, which in turn increases the frequency of collision between electrons and gas molecules. The result is more ionization, or fragmentation for organic molecules, and a higher sputtering or deposition rate. Figure 6 shows a photograph of magnetically enhanced oxygen plasma in a DC discharge system.

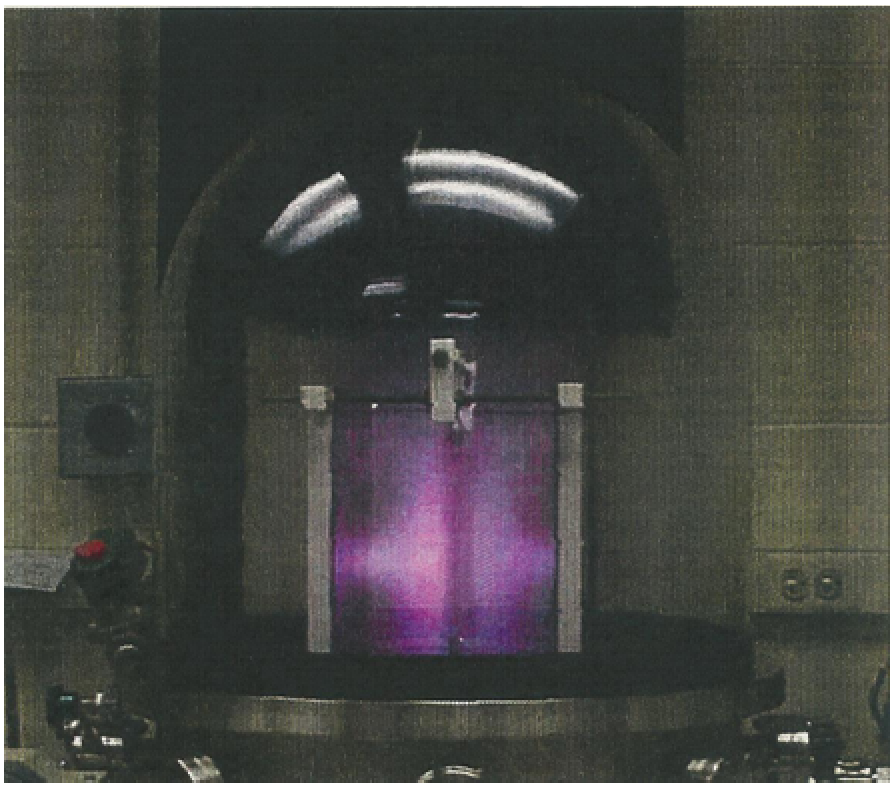

Figure 6. Photograph of DC discharge of O_2 plasma with magnetron enhanced anodes and a metal substrate as the cathode in the center.

2.3.2 Competitive Ablation and Polymerization Mechanism

Several differences between conventional polymers and plasma polymers were discussed at the beginning of this section. Another difference is the reactivity of monomers. Some monomers that are typically non-polymer forming, such as methane, can be polymerized in glow discharge. Differences in the mode of polymer formation were also mentioned. The structure of plasma polymers, unlike conventional polymers, cannot be predicted due to the complex chemical reactions taking place in the glow discharge. The modes of gas consumption depend on the monomer being used and can be considered one of three types of plasma: chemically non-reactive, chemically reactive but non-polymer forming, or chemically reactive and polymer forming [19,26].

Chemically non-reactive plasmas, like argon, can ionize materials or sputter surface materials but are not consumed. Chemically reactive but non-polymer forming plasmas, like O_2, can modify the surface by chemical etching, oxidation, interfacial recombination, etc. Deposition of polymeric materials can only occur in polymer forming plasmas.

The modes of gas consumption are described in more detail by the competitive ablation and polymerization (CAP) mechanism proposed by Yasuda et al. [27]. Shown in Figure 7, there are two means of polymerization in this mechanism. Plasma induced polymerization is initiated by the reactive species generated in polymer forming plasma. Plasma state polymerization is the mechanism for depositing polymer forming intermediates, which are caused by the simultaneous ablation of the surface and produce non-polymer forming byproducts.

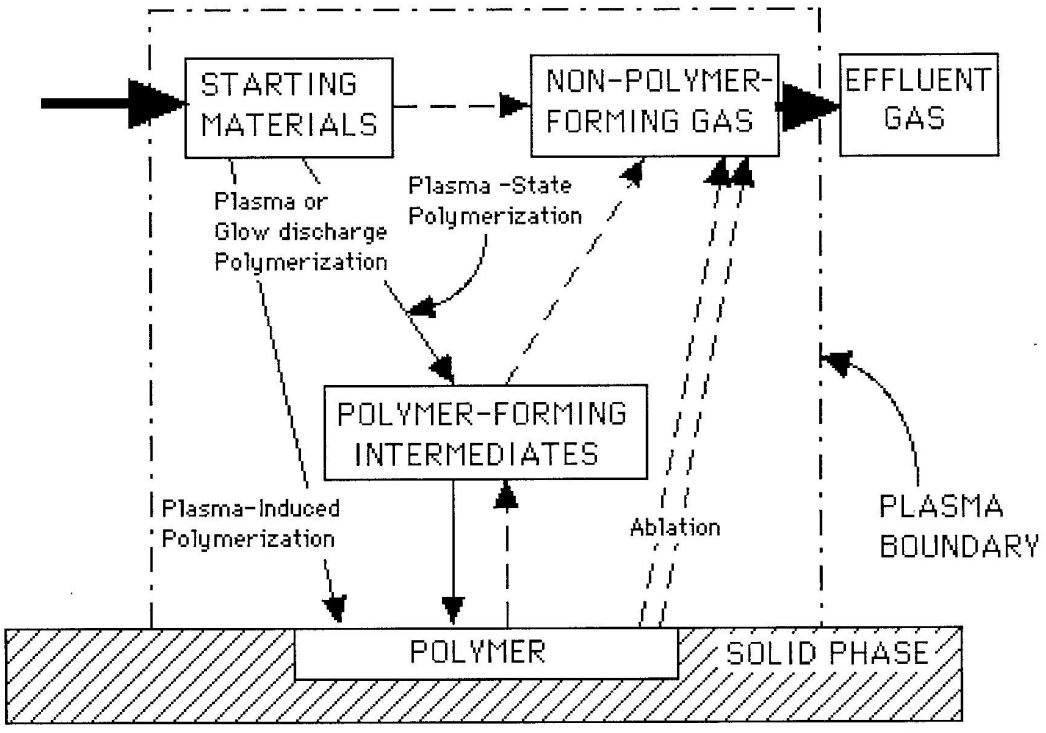

Figure 7. Competitive ablation and polymerization mechanism of glow discharge plasma [27].

When a chemically reactive and polymer forming plasma is generated, the deposition process competes with the ablation process. When a particle is sputtered off the substrate it is now in the gas phase along with the other molecules. It could combine to create another polymer forming intermediate, or redeposit if it collides with the solid surface before evacuating. This is the reason the structure of a plasma polymer is unpredictable.

2.4 Corrosion Protection of Plasma Polymers

As mentioned before, plasma polymers are ultra-thin films that are made of short segments with a high degree of branching and cross-linking giving them good barrier characteristics. They also adhere very well to a variety of substrates, including metal surfaces. Furthermore, plasma polymer films are capable of being insensitive to water which is destructive to the adhesion of thin films. They also exhibit reasonable electrical conductivity in the presence of water or oxygen, making it easy to apply an electrodeposited coating onto the coated metal [28]. These physical properties make plasma polymers an ideal choice to be used as an intermediate layer between a metal substrate and subsequent coatings.

Plasma polymerization was first shown to provide superior corrosion protection by Schreiber et al. [29] using a microwave plasma to deposit thiophene onto carbon steel. More recently, Wang [30] and Van Ooij et al. [31] demonstrated excellent corrosion resistance of cold-rolled steel (CRS) when a plasma polymerized trimethylsilane (TMS) layer followed by a cathodic E-coat was applied. Both concluded better corrosion performance versus phosphated CRS or phosphated zinc coated CRS.

2.4.1 Electrodeposited Coating

Electro-coating, also known as E-coating, is a method of organic finishing which uses electrical current to deposit the paint. The fundamental physical principle of electro-coating is that materials with opposite electrical charges attract each other. An electro-coat system applies a DC charge to a metal part immersed in a bath of oppositely charged paint particles. The paint particles are drawn to the metal part and paint is deposited on the part, forming an even, continuous film over every surface, in every crevice and corner, until the coating reaches the desired thickness. At that thickness, the film insulates the part, so attraction stops and electro-coating is complete.

Depending on the polarity of the charge, E-coating can be either anodic or cathodic. In anodic electro-coating, the metal part acts as the anode with a positive electrical charge attracting negatively charged paint particles. Likewise, the metal part has a negative charge and acts as the cathode in cathodic electro-coating. During the anodic process, small amounts of metal ions migrate into the paint film limiting the performance properties of these coating systems. Reversing the polarities for cathodic electro-coating greatly reduces this, producing high-performance coatings with excellent corrosion resistance.

2.4.2 Metal Surface Preparation

Good adhesion of the organic coating to the metal substrate is considered a major contributor to the overall corrosion resistance of a coating system. In depth studies have been done on the plasma pre-treatment process prior to plasma polymerization [32-34]. They show dramatic improvements in adhesion strength when oxides are removed from

the surface prior to depositing a plasma polymer film. The water insensitive adhesion achieved is critical for superior corrosion protection.

An oxygen cathodic pre-treatment is the oxidative chemical etching of the surface, successfully removing most organic contaminants. The steel surface is also oxidized during this process. The result of an oxygen plasma treatment is a clean steel surface containing iron oxides.

An (argon + hydrogen) cathodic pre-treatment is the sputtering of surface components by argon plasma in a reducing environment of hydrogen plasma. Sputtering combined with chemical reduction removes the metal oxides from the surface along with the organic contaminants. This treatment provides a clean, oxide-free steel surface.

Characterization of these two surface states was clearly shown by Yasuda et al. [33] using SNMS depth profiling. Two CRS samples were prepared with a TSM plasma polymer, one with oxygen pre-treatment and the other with (argon + hydrogen) pre-treatment. The SNMS depth profiles of these samples were taken from the literature and are shown in Figure 8. The panel prepared with the oxygen plasma pre-treatment (Figure 8a) shows a significant amount of oxygen at the plasma polymer/steel interface and throughout the plasma polymer film. No oxygen is found in the plasma polymer layer or at the interface for the sample that underwent the (argon + hydrogen) pre-treatment (Figure 8b).

The oxygen found throughout the plasma polymer layer can be explained by the competitive ablation polymerization (CAP) mechanism. With oxygen already on the surface, the plasma will incorporate the oxygen into the polymer forming species to be deposited. This is supported by the absence of oxygen in the plasma polymer layer of the oxide-free surface prepared by (argon + hydrogen) pre-treatment (Figure 8b). There are

Fe-C bonds, but no Fe-O bonds, present in the oxide-free plasma polymer, whereas the plasma polymer deposited onto the native oxide layer had Fe-O bonds, but no Fe-C bonds.

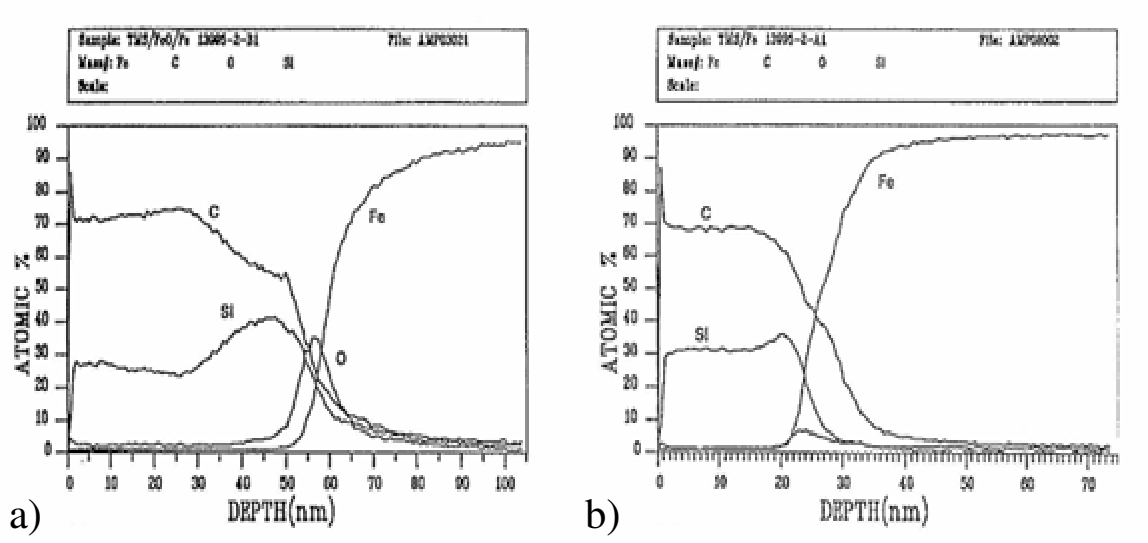

Figure 8. SNMS depth profiles [33] for a TMS plasma polymer deposited onto a) oxygen pre-treated CRS and b) (argon + hydrogen) pre-treated CRS.

The literature also showed the effects that the oxygen contained in the plasma polymer had on the cathodic electro-coating of the substrate. From SNMS depth profiles it was shown that the oxygen peak was significantly reduced when the E-coat was deposited indicating cathodic reduction is taking place during this process. It was concluded that minimizing the adverse effect of cathodic polarization drastically improves the corrosion protection of the E-coat.

2.5 Equivalent Circuit Modeling

Electrochemical Impedance Spectroscopy (EIS) is a very powerful tool for the analysis of complex electrochemical systems, specifically to characterize the quality of a

coating on a metal substrate [5-7]. EIS is a branch of AC theory that describes the response of a circuit to an alternating current as a function of frequency. AC theory is defined by the equation:

$$E = I\ Z \tag{8}$$

where E is the potential (volts), I is the current (amps), and Z is the total impedance (ohms). In alternating current (AC) circuits, the flow of electrons can be impeded by resistors, capacitors, and inductors. The impedance (Z) can be expressed as a complex number where the resistance is the real component and the imaginary component is determined by the capacitance and inductance combined. EIS measures the complex impedance of an electrochemical cell over a wide range of AC frequencies.

In a DC circuit (AC circuit where the frequency equals 0 Hz) only resistors impede the flow of electrons. For DC theory, Equation 8 is reduced to:

$$E = I\ R \tag{9}$$

which is Ohm's Law where R is the resistance (ohms).

EIS spectra analysis can be very complicated because the impedance of the system usually depends on more than one cell element. For this reason, EIS data is commonly analyzed by fitting it to an equivalent electrical circuit model made up of the common electrical components (resistors, capacitors, or inductors) [35-39]. Both serial and parallel combinations of these components occur to generate a network that will accurately describe the physical electrochemistry of the system. In a physical model, each of the model's components is postulated to come from a physical process in the electrochemical cell. The choice of which physical model applies to a given cell is made from knowledge of the cell's physical characteristics.

One of the simplest models is the Randles cell shown in Figure 9, which models the interface of a metal surface in contact with an electrolyte [36,37]. The solution resistance between the reference electrode and the working electrode is often a significant factor in the impedance of an electrochemical cell and is accounted for using R_s. At the electrode/electrolyte interface there exists an electrical double layer. This double layer is formed as ions from the solution "stick on" the electrode surface creating an insulator between the electrode charges and ion charges. Even though very small, on the order of angstroms, separated charges form a capacitor. In the Randles circuit, the double layer capacitance (C_{dl}) is in parallel with the charge transfer resistance (R_{ct}). This resistance is due to another process at this interface. When the metal is in contact with the electrolyte, electrons enter the metal and metal ions diffuse into the electrolyte, transferring the charge. Most electrochemical systems are far more complicated than what the Randles cell models. It is, however, a starting point for other more complex models.

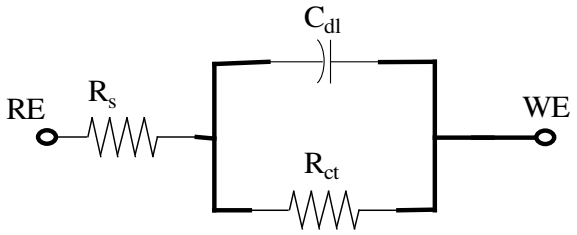

Figure 9. Schematic diagram for the Randles circuit. RE = reference electrode; WE = working electrode; R_s = electrolyte solution resistance; C_{dl} = double layer capacitance; R_{ct} = charge transfer resistance.

Derived from the Randles cell, the circuit model shown in Figure 10 is commonly used to represent coated metal systems [38,39]. A coating capacitance (C_c) is included to account for the insulation that the intact coating provides. Over time, water can penetrate into the coating and form a liquid/metal interface under the coating. The coating

resistance (R_c), or pore resistance, is the resistance of ion conducting paths that develop in the coating. On the metal surface, if an area of the coating delaminates, a pool of electrolyte solution will form. The interface this pool of solution forms with the metal surface is modeled like the electrolyte/metal interface in the Randles cell, with a charge transfer resistance and double layer capacitance in parallel.

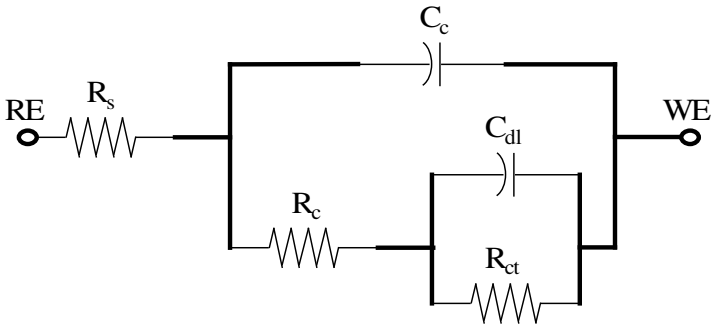

Figure 10. Schematic diagram of an equivalent circuit used to describe coated metal systems. RE = reference electrode; WE = working electrode; R_s = electrolyte solution resistance; C_c = capacitance associated with the coating; R_c = resistance associated with the coating; C_{dl} = double layer capacitance; R_{ct} = charge transfer resistance.

3. EXPERIMENTAL

3.1 Materials

Cold rolled steel (CRS) panels (15 cm x 10 cm) used for this study were purchased from Advanced Coatings Technology, Inc. (Hillsdale, MI). The panels remained wrapped in a vapor cloth to prevent rusting until they were ready for use.

The gases used for the plasma pretreatment and plasma polymerization process were argon of 99% purity, hydrogen of 99% purity, and oxygen of 99.9% purity all procured from Airgas. Trimethylsilane (TMS) of 97% purity was procured from Lancaster Synthesis, Inc. (Windham, NH). All gases were used with no further purification.

The electro-coat (E-coat) used was a mixture of 44 wt % resin emulsion (BASF U32CD033A), 8 wt % paste (BASF U32AD290), 48 wt % DI water and 4 vol % additive (BASF 20CD0043). All of these materials were supplied by Boeing (Boeing Co., St. Louis, MO). The spray primer was water borne Spraylat (Spraylat Corp., Chicago, IL) consisting of 3 parts base component EWAE118A and 1 part activator EWAE118B.

3.2 Plasma Reactor System

The reactor setup, shown in Figure 11 (diagram) and Figure 12 (photograph), was 75 liters with an MDX-1K Magnetron Drive power supply (Advanced Energy Industries, Inc.) used as the DC plasma generator. Two stainless steel plates (25.4 x 25.4 x 0.16 cm), insulated with ceramic bars, were placed 15.5 cm apart and used as anodes in the plasma system. The anodes were magnetron enhanced by placing eight 1000 Gauss bar magnets (1.2 x 0.6 x 5.0 cm) in a spoke formation on the back of the plates with the

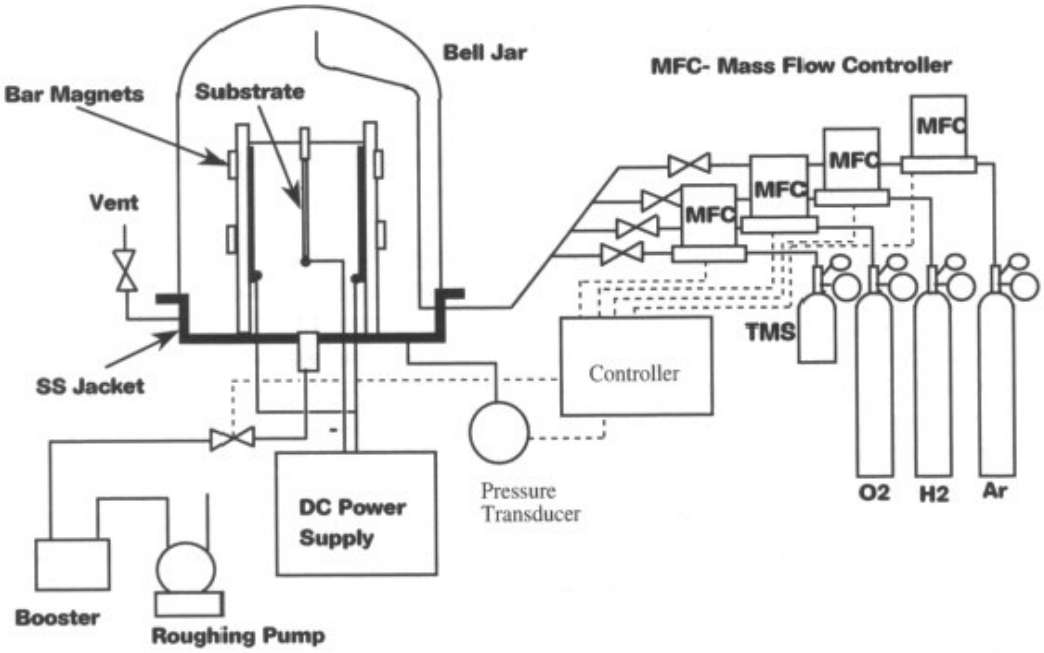

Figure 11. Schematic diagram of the DC bell jar reactor system.

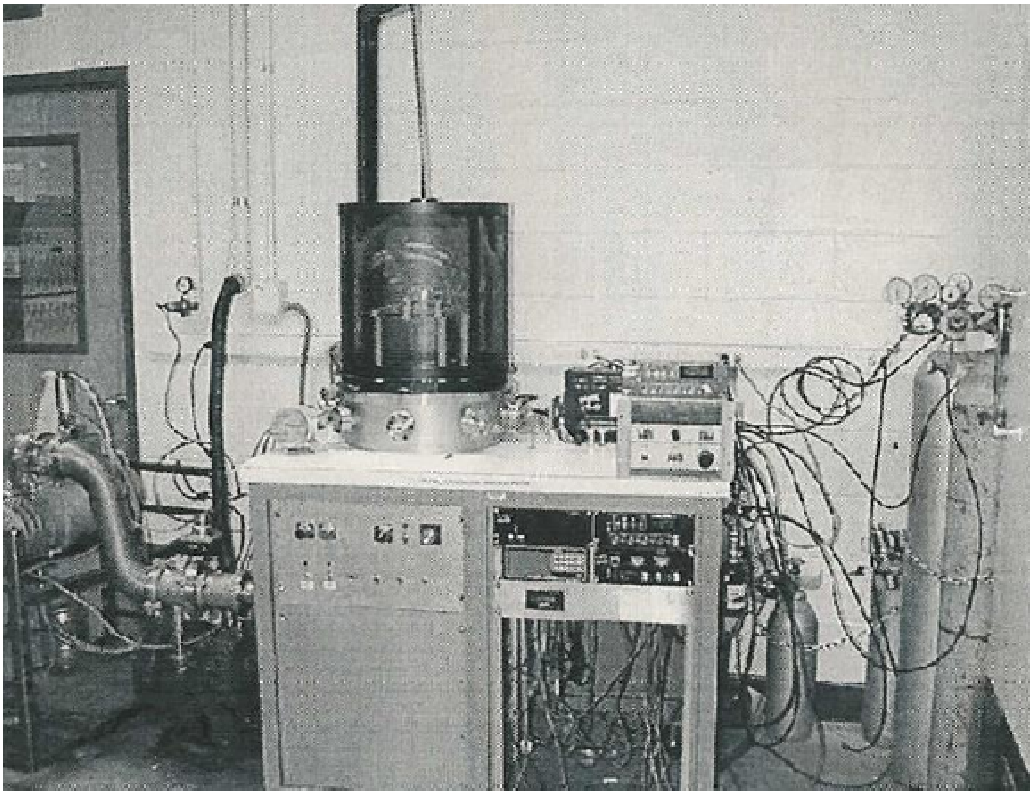

Figure 12. Photograph of the DC bell jar reactor system.

south poles facing the center. An iron plate ring (22.86 cm O.D. and 17.78 cm I.D.) and a circular iron plate (10.16 cm diameter) were placed between the magnets and the electrode to produce a uniform magnetic ring. The CRS substrate was placed in the center of the anodes and used as the cathode.

The reactor chamber was pumped down to a pressure of approximately 2 mTorr using a roughing pump (Sargent-Welch Duo Seal 1370 rotary pump) and a booster pump (Edward 250H Mechanical Booster pump) in series as the vacuum unit. This vacuum pump system was connected to the bottom of the reactor chamber. Isolation of the reactor chamber from the pumping line was achieved by an on/off valve located between the pumps and the reactor chamber. The desired gas was then fed into the reactor. The flow rates were monitored by a MKS mass flow meter (Model 247 C) and the gas pressure in the chamber was controlled by a MKS pressure controller (Model 252 A). Once the system pressure was stable, the DC power was applied for the desired operation conditions. For multiple treatments, the system pressure was brought back to 2 mTorr between treatments to remove the monomer gases just used. After completion, the residual gases were pumped out of the reactor chamber and the vacuum was released.

3.3 Sample Preparation

The cold rolled steel (CRS) panels were received with several contaminants on the surface. They were cleaned prior to use by acetone wiping with Kimwipes to remove ink stamp marks and other loose organic matter from the surface. A small piece of silicon wafer was mounted on the panel using conductive silver paint in order to measure the coating thickness. The CRS panel was hung in the bell jar reactor system using an insulated clip. The plasma pretreatment and plasma polymerization conditions are shown

in Table 1. Subsequent plasma treatments done in situ are separated with a "/", therefore the sample (AH)/T would have a cathodic (argon + hydrogen) pretreatment followed by the deposition of a TMS plasma polymer before being removed from the reactor.

Table 1. Conditions for Plasma Treatments

Symbol	Treatment	Flow Rate (sccm)	System Pressure (mTorr)	Power (Watts)	Treatment Time (min)
(O)	O_2	2	50	5	2
(AH)	$Ar + H_2$	1 + 2	50	40	10
T	TMS	1	50	5	0.5 – 2.5

Once removed, with the exception of those intended for linear polarization measurements, the samples were immediately coated with either the spray paint or E-coat primer. The primer thickness was controlled to approximately 25 µm for all samples. The samples prepared for the linear polarization measurement were put in a sample bag and stored in a desiccator until tested.

3.3.1 Spray Painted Primer

To apply the primer, the panels were laid flat and slightly raised from the hood surface. The nozzle was held directly above the panel approximately six inches away. Two slow, smooth passes using 30 psi air pressure were made to completely cover that side of the panel. The sample was allowed to air-dry for 30 minutes before curing in the oven at 350° F for 20 minutes. Samples to be used in the corrosion (GM scab) test had the uncoated side covered with insulating tape to reduce corrosion away from the area of focus.

3.3.2 Electrocoated Primer

A one gallon electro-coat (E-coat) bath contained in a 3.8 L Pyrex® brand glass jar (14 cm x 16 cm x 27 cm) was used for the electro-coating. The bath remained well mixed by using a TEFLON® coated magnetic stirrer (Fisher 11-498-7S) that had length of 3.0 cm and a diameter of 0.65 cm. The sample was immersed into the bath and connected as the cathode along with a stainless steel strip (4 cm x 25 cm x 0.1 cm) used as the anode. The electrodes were connected to a Darrah Digital® 3350 DC power source (Darrah Electric Co., Cleveland, OH) for the electro deposition.

For the electro deposition, the panel was hung by a paper clip and immersed into the electro-coat bath. A timer on the DC power supply was set for two minutes, and the power was turned on. Starting at zero, the voltage was slowly increased. The current was monitored and not allowed to exceed 1 ampere. In approximately 20 seconds, the current dropped sharply and the voltage was raised to 250 volts for the remaining time. Upon completion, the sample was rinsed with DI water and air-dried for 30 minutes. It was then oven cured at 350° F for 15 minutes.

3.4 Testing Methods

3.4.1 Thickness Measurements

The thickness and refractive index of the plasma polymer films were measured from a silicone wafer using a null-seeking type AutoEL-II Automatic Ellipsometer (Rudolph Research Corporation, Flanders, NJ) with a 632.8 nm helium-neon laser light source. The silicone wafer was attached to the substrate with conductive silver paint.

An Elcometer® 355 (Elcometer Inc., Rochester Hills, Michigan) with a non-ferrous probe was used to measure the organic coating thickness, spray paint and E-coat.

3.4.2 Tape Test

Adhesion testing was done using a standard tape test (ASTM D3359). Painted samples were scribed with a razor blade to expose the metal surface in the shape of a grid. It was done by scribing 11 vertical and 11 horizontal lines making a surface of approximately 2 cm^2. Tape was then pressed onto this grid and removed with a quick pull. A handheld microscope was used to determine the amount of paint removed from the surface. A grade of 0-5 was given with 5 being complete adhesion, and 0 being total removal of the paint. This was done dry and after boiling in water for 1, 4, and 8 hours.

3.4.3 GM Scab Test

To test the performance of the coatings against corrosion, samples were subjected to the accelerated corrosion test GM 140-F (333-K), known as the GM scab test. Two sets of painted samples were subject to a cyclic procedure over a period of four weeks. On Monday-Friday the panels were soaked in a 5% salt solution for 15 minutes. They were rinsed with DI water and air-dried for an additional 1 hour and 15 minutes. Then the panels were placed in a humidity chamber maintained at 60^{o}C and 85% R.H. Saturday and Sunday the panels were kept in the humid environment.

One set of samples was used for EIS measurements. A measurement was taken prior to starting the GM Scab test followed by one every Monday during the testing period for a total of five measurements.

The other samples were scribed on the surface to facilitate a damaged coating. The X-shaped scribe was made using a diamond tip probe on computer controlled equipment. The scribe depth was set to 30 µm to ensure the bare substrate was exposed. After completion of the GM Scab test, the scribed panels were covered with Turco 5469

stripper solution (Aviall Co., Dallas, TX) to remove the organic coating, either spray paint or E-coat. The stripped panels were rinsed with DI water and visually observed. These samples were used to calculate the corrosion widths of the different treatments.

3.4.4 Corrosion Width

The corrosion performance was quantified using OPTIMAS 6.1 image analysis software to calculate the corroded area. The scribed panels were first scanned into the computer using an HP DeskScan II scanner. The image was adjusted to have a total area of 47.5 cm^2 centered at the intersection of the scribed X. The total length of the scribe was 22.0 cm. For accurate analysis, the images were scanned at a 450x900-pixel resolution.

The image with known dimensions was then imported into the OPTIMAS software window. The corroded area and the entire image area were outlined using the area morphometry method. The corroded, un-corroded, and total areas are reported from which the percent corroded area and subsequently the actual corroded area were calculated. The corrosion width was then determined by divided the corroded area by the total scribe length within the scanned area.

3.4.5 Linear Polarization

The linear polarization resistance measurements were done using an EG&G Instruments Potentiostat/Galvanostat Model 273A controlled by 352 SoftCorr™ III Corrosion Measurement Software. Insulating tape was used to mask off an area of 3x3 cm^2 on the CRS panel, which was used as the working electrode. The reference electrode was Ag/AgCl (0.197 V vs. NHE), and the counter electrode was a graphite rod. The

electrolyte was a salt solution with a composition of 0.5 wt.% NaCl and 0.35 wt.% $(NH_4)_2SO_4$. This solution is slightly modified from a dilute Harrison solution, which has a 0.05 wt.% of NaCl.

3.4.6 Electrochemical Impedance Spectroscopy

EIS measurements are done using the EG&G Instruments Potentiostat/Galvanostat Model 273A which is run by the computer. Measurements were taken from 0.1 Hz to 5 kHz with 10 mV sine wave potential collecting five points per decade. The cell is set up with the sample as the working electrode, a SCE for the reference electrode, and a thin platinum wire for the counter electrode. A glass bell-shaped tube with a fitted rubber o-ring was clamped onto the surface of the sample and filled with the electrolyte solution. The electrolyte solution is a modified dilute Harrison solution (0.5% NaCl, 0.35% $(NH4)_2SO_4$ and was in contact with the working electrode for about 30 minutes prior to starting the experiment.

3.4.7 Equivalent Circuit Modeling

The frequency and impedance, real and imaginary components, from the EIS data were imported into the equivalent circuit modeling software ZSimpWin (Princeton Applied Research). Any one of numerous plots can be displayed, but the Bode plot including the impedance values and phase angles was preferred. An electrical circuit was either chosen from a list or manually entered. The ZSimpWin software would run a series of iterations using the specified circuit elements and compare the simulated data to the measured EIS data. The ability of the equivalent circuit to model the data was determined by the plots visual fit and the chi-squared value calculated by the software.

4. RESULTS AND DISCUSSION

The extent of corrosion protection from a coating applied to a metal substrate is determined by the coating system as a whole. Each layer making up the coating is interrelated and cannot be chosen solely on its performance as a corrosion barrier.

The three major factors that determine the overall effectiveness of the coating are: (1) the barrier characteristics of the primer, (2) good adhesion between the primer and metal substrate, and (3) the surface state of the substrate.

Corrosion may occur from two different mechanisms. If water can permeate through the primer layer, it can form pools at the primer/substrate interface. This allows for salt intrusion to take place and promote corrosion. This pitting corrosion proceeds when the coating is undamaged. The second mechanism describes corrosive behavior at sites where the coating is damaged and the substrate is exposed. Along with inevitable corrosion at the bare site, delaminating of the adjacent coating may occur, increasing the area subject to corrosion.

The coating system used in this investigation is a primer film/plasma polymer layer/steel substrate. The primer and plasma polymer layers were varied in an attempt to achieve the best overall coating system. Two primers were used for the outer most coating of the system. A spray painted primer was applied via air spray, and a cathodic E-coat electrochemically bonded to the surface. Two plasma treatments were also used in this study. A cathodic oxygen plasma treatment was used to clean the surface of the substrate providing a good base for the plasma polymer to form [40,41]. A cathodic (argon + hydrogen) plasma treatment was used on other samples to rid the surface of the oxide layer [32-34]. All samples underwent a TMS plasma polymerization in situ of the

plasma pre-treatment which has been shown to provide excellent corrosion resistance [22,31-34].

4.1 Linear Polarization Resistance

The rate of an electrochemical reaction in an unpainted metal/electrolyte system and its sensitivity to current flow can be quantified by its polarization resistance (R_p) value [24,42-43]. A small amount of current flow is evident from higher polarization resistance values. This is attributed to the sample having a greater corrosion resistance.

Conditions for the plasma pretreatments were based on the literature [33] and are shown in Table 1 (Section 3.3) along with the TMS plasma polymerization conditions. Figure 13a shows the R_p values for TMS plasma polymer coated steel panels that underwent oxygen plasma and (argon + hydrogen) plasma surface cleaning. Without depositing a TMS film, there was little difference between the plasma pretreatments alone (a control panel with no pretreatment had an R_p value of 135 ohms). The corrosion resistance of the oxygen and (argon + hydrogen) cleaned panels increased dramatically with TMS treatment time and both reached a maximum value around two minutes.

The thickness of the plasma polymer layer is important. If a critical thickness is exceeded, the coating will begin to buckle and possibly crack. From Figure 13b it can be seen that the ideal thickness for the TMS layer deposited on the (argon + hydrogen) cleaned samples is approximately 75 nm. It is also shown that the oxygen treated samples require a much thicker TMS layer to have any improvement. For the same two-minute treatment time (Figure 13a), the ideal thickness on the oxygen treated samples is about 120 nm. This is almost twice as thick as the (argon + hydrogen) treated panels, which will result in much weaker adhesive and cohesive strength.

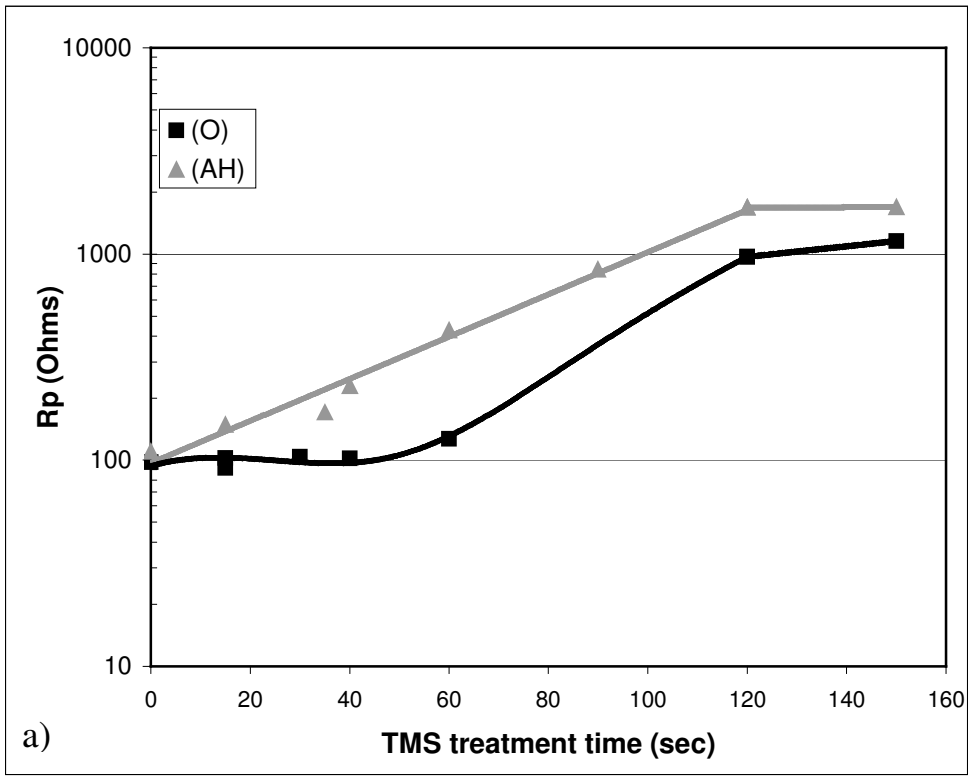

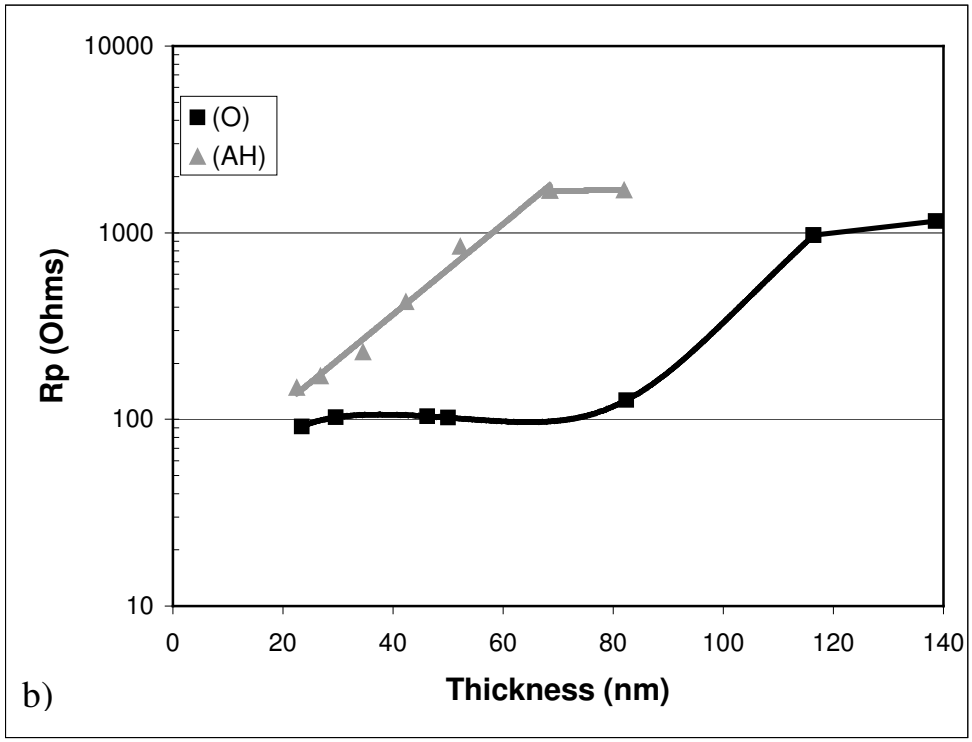

Figure 13. Linear polarization resistance plotted against a) TMS treatment time and b) TMS film thickness with (argon + hydrogen) pretreatment and oxygen pretreatment.

The thickness growth rate and refractive indexes for the two treatments are shown in Figure 14. Although the growth rate is lower, the larger refractive index for the (argon + hydrogen) treated panels, around two, shows that the plasma polymer layer is much denser than the oxygen treated samples. The more cross-linked network of hydrophobic particles will provide a better foundation for water insensitive adhesion to the primer layer. This is a very important characteristic, as discussed earlier.

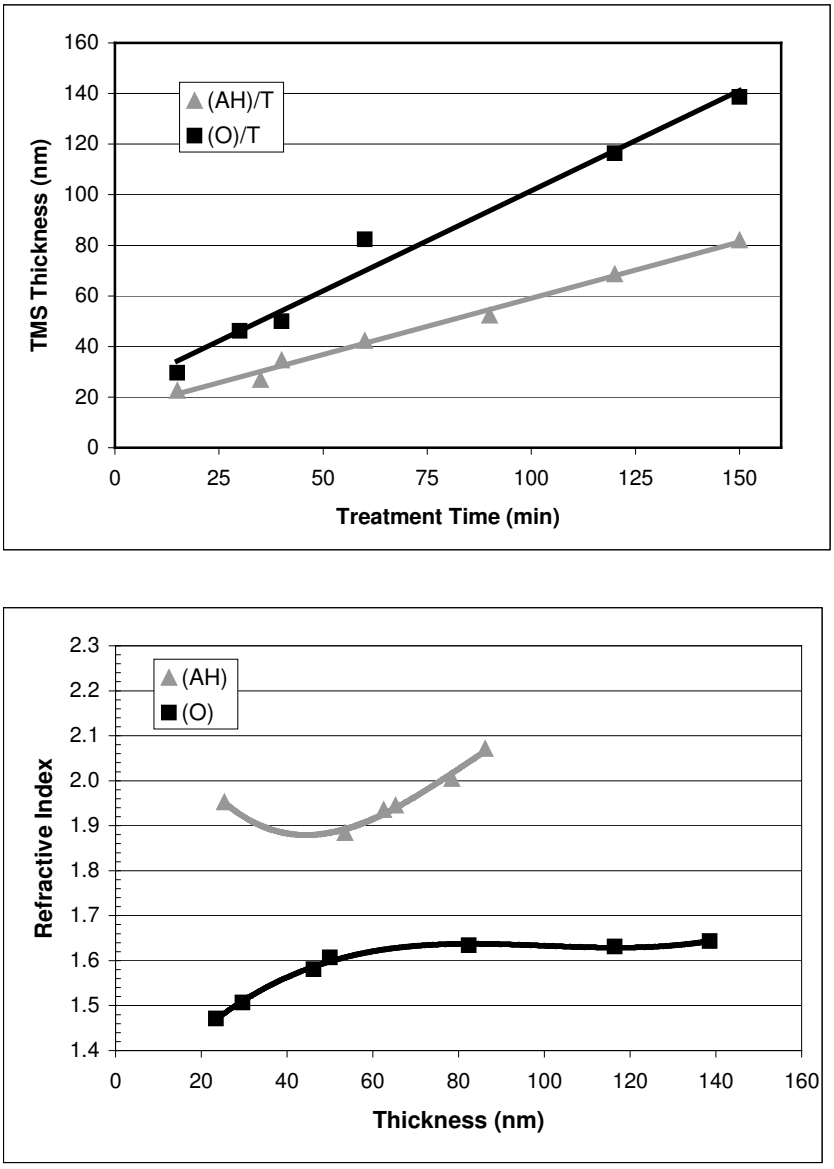

Figure 14. TMS film thickness growth rate and refractive index values versus the TMS film thickness for the samples with (argon + hydrogen) pretreatment and oxygen pretreatment.

Even though the increased amount of cross-linking will result in better adhesion, the polymer film will be under a greater amount of internal stress because the refractive index is directly proportional to the internal stress. For the (argon + hydrogen) treated samples, the optimized film thickness of 75 nm produces a refractive index of approximately 2.0. Exceeding this value likely puts too much stress on the polymer chains, resulting in reduced coating performance for thicker polymer films.

4.2 Adhesion of Primer

Four samples were prepared for the following tests using the same TMS deposition conditions (1 sccm; 50 mTorr pressure; 5 Watts; and 2 min treatment time) chosen from the best linear polarization results. Following the TMS polymerization, two different primers were used for the outer-most layer of the coating system. Two additional samples without any plasma treatment were used as controls, one spray painted and one E-coated. The treatments for the six samples prepared are shown in Table 2. They were tested for their corrosion resistance capabilities and related to adhesion characteristics.

Table 2. Sample Identification for the Coated Steel Substrates

Sample	Treatment	Primer
A	None	Spray Paint
B	(O)/T	Spray Paint
C	(AH)/T	Spray Paint
D	None	E-coat
E	(O)/T	E-coat
F	(AH)/T	E-coat

The adhesion was quantified using a tape test under dry conditions and subjected to boiling water up to 8 hours to test wet adhesion. It is shown in Table 3 that all three samples with the spray painted primer demonstrated good dry adhesion, but delaminate

quickly in boiling water. The (argon + hydrogen) treated panel was the only one that did not completely delaminate before 8 hours.

The tape test results for the E-coated samples are also shown in Table 3. Each of these exhibited excellent wet and dry adhesion. The oxygen cleaned panel started to delaminate at 4 hours and continued to get worse. After immersed in boiling water for 8 hours, the substrate treated with (argon + hydrogen) plasma remained completely covered with the primer.

Table 3. Tape Test Results for Wet and Dry Adhesion

Sample	Dry	1 hour	4 hours	8 hours
A	4	1	0	0
B	4	2	0	0
C	4	3	1	1
D	5	5	3	2
E	5	5	4	2
F	5	5	5	5

Scanned images of samples with the spray painted primer following the GM scab test are shown in Figure 15. The images were scanned after removal of the primer layer with Turco stripper solution to reveal the bare substrate. It can be seen that a significant amount of corrosion propagated from the damaged site (scribed X). It is also evident that the plasma treatment determined the degree of corrosion.

The amount of corrosion on the E-coated samples, although to a much lesser degree, was still influenced by the plasma treatment. Scanned images of these samples are shown in Figure 16. Common to the spray painted samples, the least amount of corrosion is observed for the (argon + hydrogen) pretreated samples.

The amount of corrosion that propagated from the scribe (corrosion width) was determined from imaging software. This value, shown in Figure 17, is used to quantify the performance of the coating systems that was visually observed from the images.

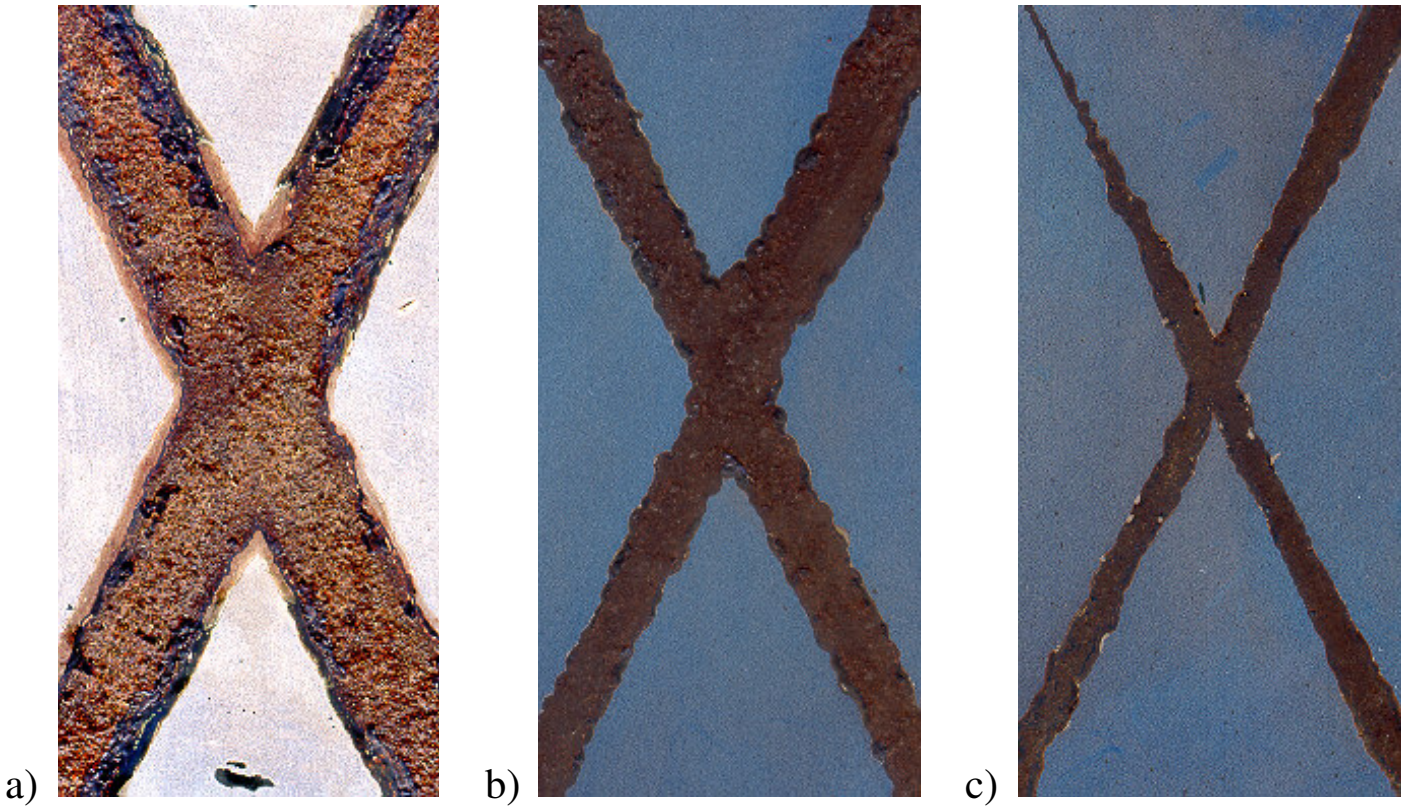

Figure 15. Scanned images of the spray painted CRS panels following the GM scab test: a) sample A, b) sample B, and c) sample C.

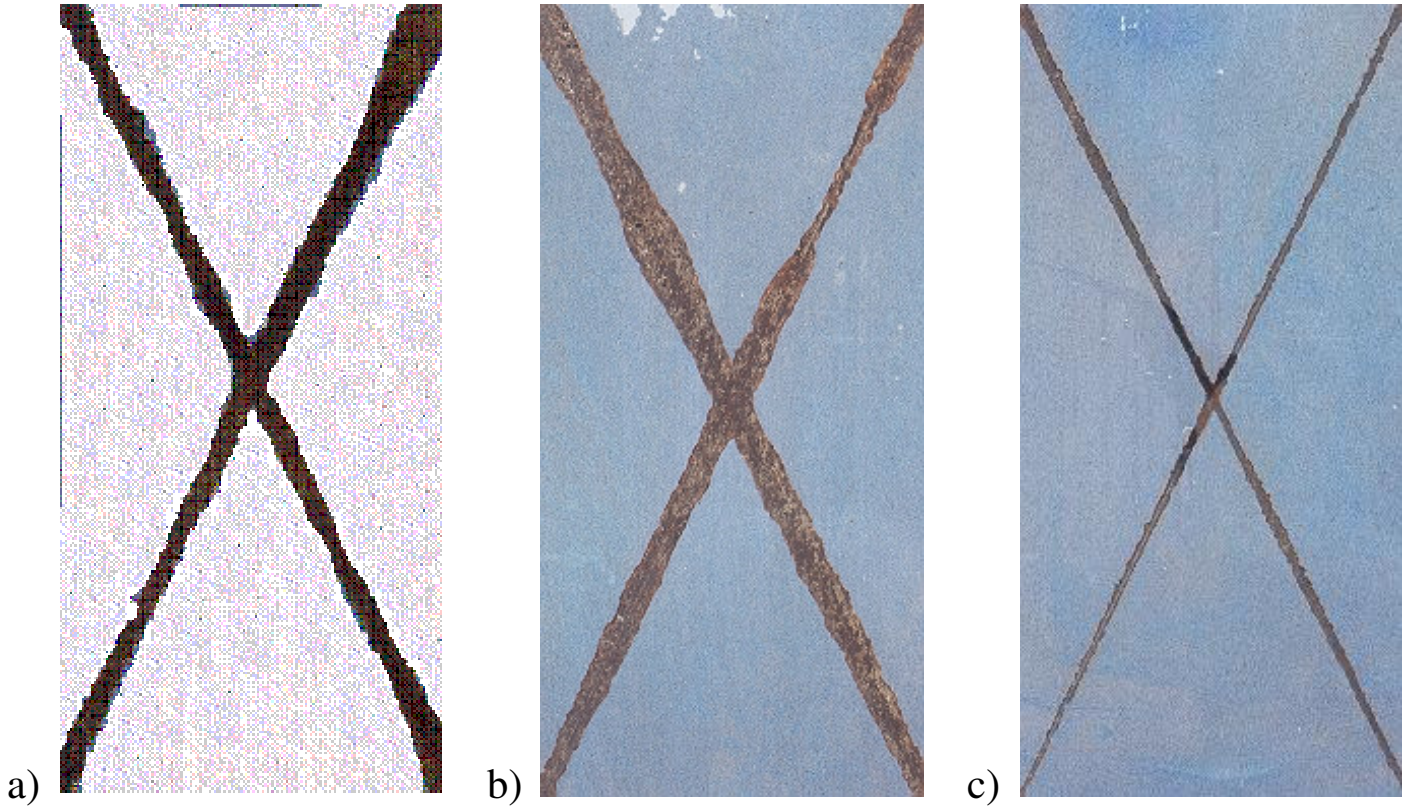

Figure 16. Scanned images of the E-coated CRS panels following the GM scab test: a) sample D, b) sample E, and c) sample F.

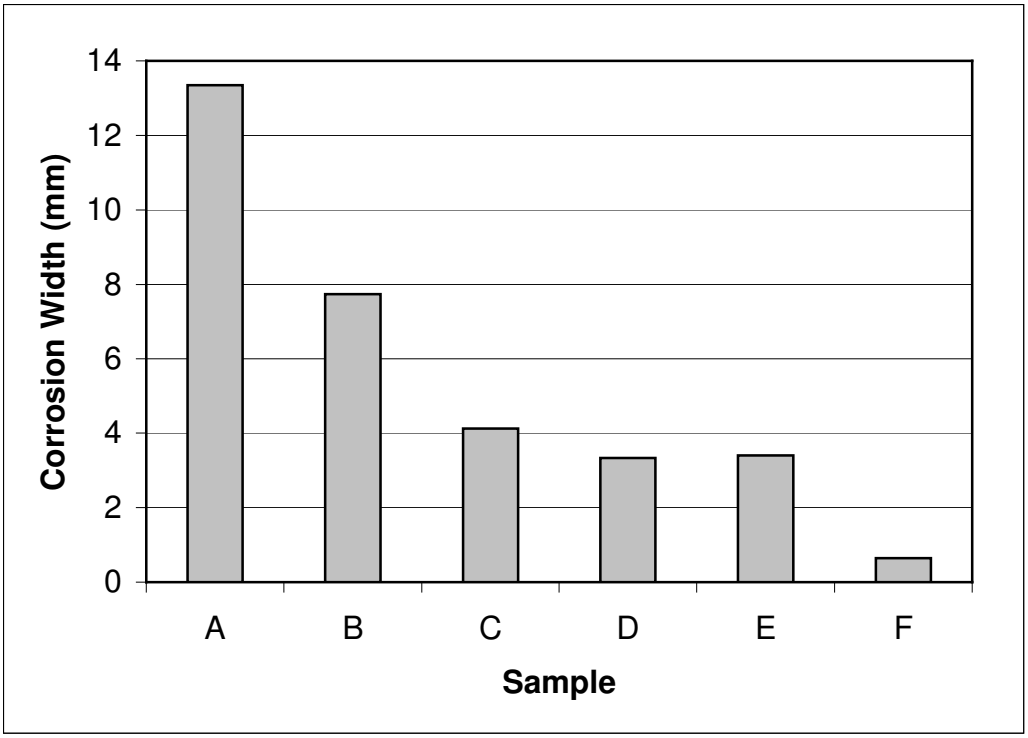

Figure 17. Corrosion width measurements for the spray painted (A-C) and E-coated (D-F) samples.

The most obvious statement is that the E-coat panels significantly outperformed the spray painted panels. This correlates well with the results from the tape test where the E-coat primer had a much stronger adhesion to the steel substrate. The tape test also revealed that the (argon + hydrogen) treatment resulted in better adhesion and subsequently better corrosion protection. This is definitely the case as it is shown in Table 3. There is a dramatic improvement of corrosion protection from the oxygen treated panel to the (argon + hydrogen) treated panel. This observation agrees with previous work investigating the affect of oxides on coated CRS discussed in Section 2.4.2 of this paper. It has been shown that coated oxide-free CRS is much more corrosion resistant than coated CRS with oxides on the surface emphasizing the importance of an oxide–free substrate on the overall coating performance.

4.3 Electrochemical Impedance Spectroscopy

Electrochemical Impedance Spectroscopy (EIS), like linear polarization resistance, is a valuable technique used in determining the extent of corrosion protection a coating system can provide. In the previous section, linear polarization was used to compare different surface treatments and their influence on the overall coating system. This technique, however, is limited to testing bare metals. It is deficient for metals that are coated with an electrically insulating material such as paint. EIS solves this problem and is a powerful tool to study a coated metal substrate. EIS methods can detect deterioration at coating/metal interfaces well before defects become visible. Changes in electrical properties determined by EIS experiments closely resemble long-term performance of the coating, making it a useful technique to predict the effectiveness of a coating over time.

The most common way to illustrate the coating performance is in the form of a Bode plot (impedance vs. frequency). The impedance (|Z|) recorded at low frequency (0.1 Hz) quantifies the overall performance of the coating system. In general, coatings with $|Z| > 10^8$ ohms at 0.1 Hz are considered to provide excellent protection, and coating with $|Z| < 10^6$ ohms are considered to provide poor protection.

EIS Bode plots for each week during the corrosion (GM scab) test, including the initial plot, for the spray painted samples are shown in Figure 18. Common to all of the painted samples is a dramatic decline in the impedance modulus at 0.1 Hz within the first week of the scab test. The two samples with a TMS plasma polymer layer (samples B and C) initially showed good barrier characteristics: both having an impedance value greater than 10^8 ohms. After being exposed to humid conditions, however, the

impedance modulus for all three samples quickly dropped 2 orders of magnitude where it remained fairly constant at 10^6 ohms for the duration of the testing period.

The Bode plots for the E-coated samples are shown in Figure 19. The control had a slight drop in impedance modulus at 0.1 Hz, but remained between 10^6 and 10^8 ohms, which would be considered moderate coating performance. There is a significant improvement in corrosion protection for the two samples with a TMS plasma polymer layer (samples E and F). With an initial value near 10^9 ohms, the impedance modulus for the oxygen treated panel only dropped approximately one order of magnitude. This good coating system is only outperformed by the sample with an oxide-free surface. The (argon + hydrogen) treated panel demonstrates outstanding corrosion protection by having a straight line to an impedance of 10^9 ohms that remained unchanged for the entire testing period. The EIS Bode plots for the four-week experiment suggest that there is no degradation in coating performance over an extended period of time.

For simplification, the change in impedance modulus at 0.1 Hz is shown in Figure 20 for all six samples. This plot clearly shows the importance of good adhesion of the primer to the substrate. All three samples that contained the spray painted primer, which had very poor adhesion determined from the tape test, had drastic impedance modulus declines after one week in the accelerated corrosion test. They eventually all converged below 10^6 ohms indicating poor corrosion protection. The similar impedance values for these samples suggest there is a common factor limiting the corrosion protection. The key variable must be the spray painted topcoat, because each sample has different underlying layers. For this coating system, the surface treatments appear to be irrelevant due to the poor adhesion and weak barrier performance of the spray painted primer.

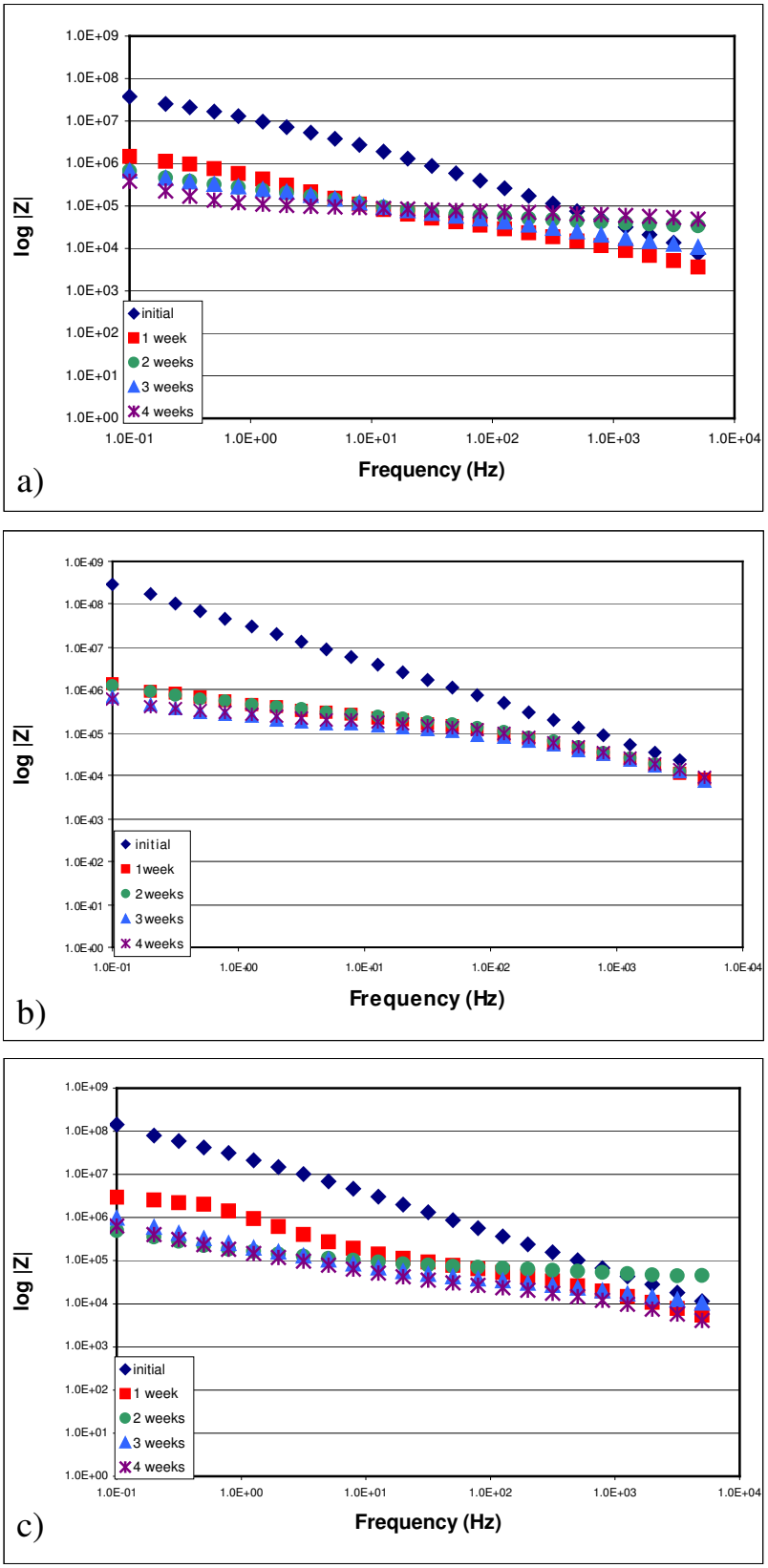

Figure 18. EIS Bode plots during the GM scab test for the spray painted samples: a) sample A, b) sample B, and c) sample C.

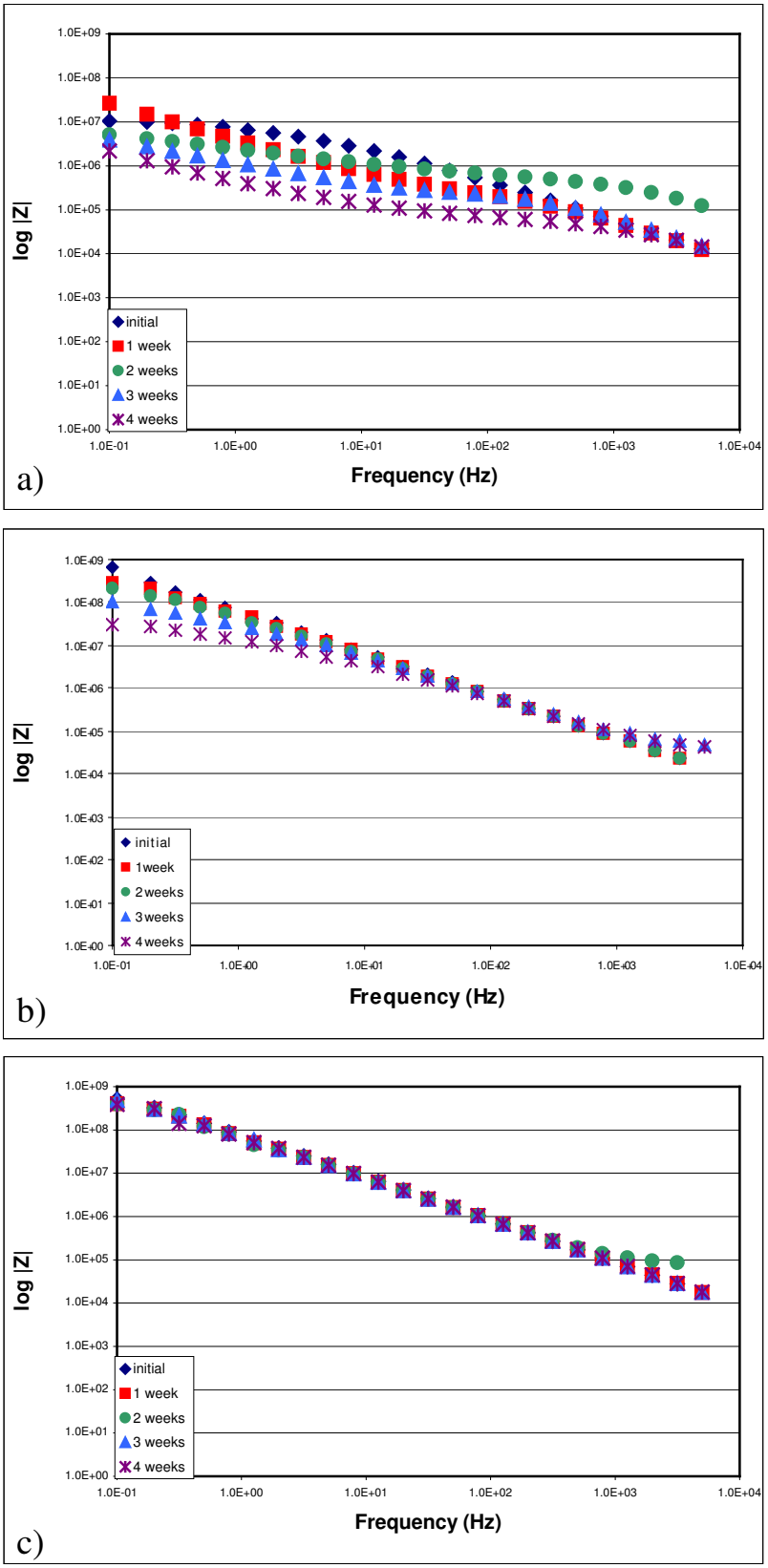

Figure 19. EIS Bode plots during the GM scab test for the E-coated samples: a) sample D, b) sample E, and c) sample F.

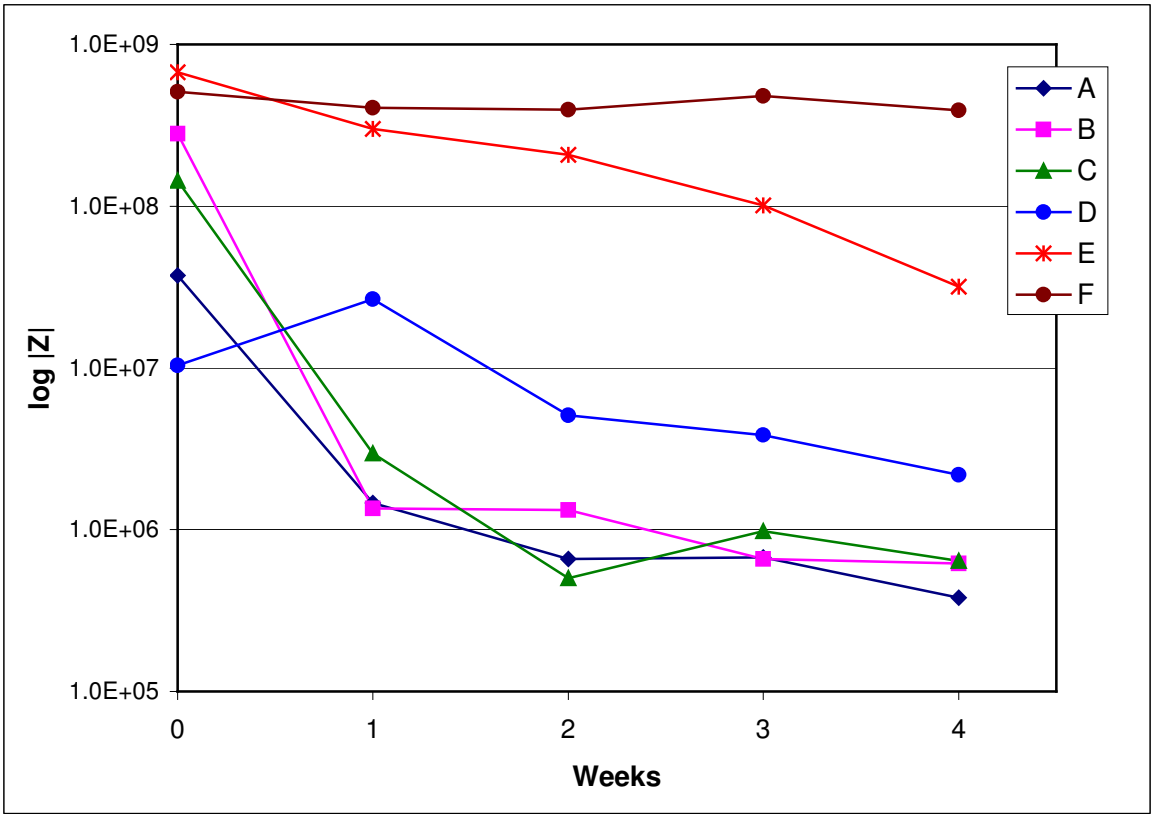

Figure 20. Value of the impedance at the lowest frequency (0.1 Hz) for all of the samples throughout the four-week corrosion (GM scab) test.

The E-coated samples all performed much better. Two obvious observations are; the E-coated samples had very little, if any, coating degradation in the first week of the scab test, and they all had much higher impedance values after four weeks. There was only a slight drop in impedance modulus at low frequency for samples D and E, and the plot shows a virtually horizontal line for the E-coat/TMS plasma polymer/oxide-free steel panel (sample F).

Unlike the spray painted samples which were not distinguishable, the performance of the ones prepared with the E-coat are influenced by the surface treatments prior to the applying the topcoat. The TMS plasma polymer proved to be an important element in the coating system shown by the significantly larger impedance values for samples E and F than the control (sample D). The initial impedance values for these two are comparable to each other and larger than the other samples. Sample F, however, maintained this high value, whereas sample E has a steady decline, resulting in some separation at the end of the testing period. This can be attributed to the conditions of the plasma cleaning each underwent. Consistent with the data from the previous section, the oxide-free panel produced via an (argon + hydrogen) plasma treatment (sample F), performed better than the oxygen cleaned panel (sample E).

4.4 Modeling EIS Data

Although much can be learned from the EIS data just presented, the capabilities of this technique go beyond what has been utilized to this point. Studying the impedance data over a set frequency range can be very informative about the coating system. The system being tested, however, can be modeled as a collection of electronic elements. The proper amount and orientation of these elements will produce a frequency response

similar to that measured by the EIS experiment. Associating the model elements with the individual component layers will generate more detailed information about the corrosion protection of the coating system. It is then possible to look inside the "black box" and determine the dominant factors to the drop in impedance modulus observed in the Bode plots.

The EIS data was evaluated using the ZSimpWin software program. The selected model would first have to have an acceptable fit (low chi-squared value) before any further investigation would take place. This, however, did not ensure an accurate model to represent the coating system. The calculated parameters had to be analyzed to determine if there was a correlation to the actual corroding state of the system.

The literature discussed a general equivalent circuit used to model coated metal systems [38,39]. Shown in Figure 21, this model (Model 1) uses two parameters to describe the corrosion process at the coating/steel interface; the charge transfer resistance (R_{ct}) and the double layer capacitance (C_{dl}). Two parameters are also used to describe the coating (R_c and C_c). R_c and C_c have been used to describe a painted metal as well as a metal coated with a plasma polymer. The interface engineered systems in this study incorporate both of these layers making them slightly more complicated. This model simulated the EIS data well, but after reviewing the parameter values there was no relationship between the model parameters and the actual conditions of the coating. Even though Model 1 was not chosen to represent these coating systems, it was used as a guideline in attempting to generate an accurate model.

Another model influential to this study was one developed by Yasuda et al. [8], shown in Figure 22 (Model 2). It utilizes the concept that the interfacial behavior results from the surface states of the two materials in contact. There are, therefore, four circuit

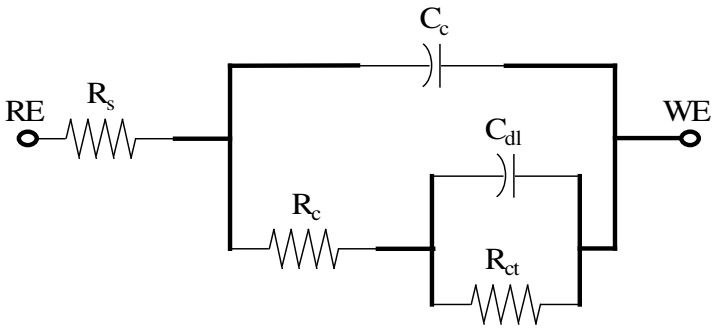

Figure 21. Schematic diagram of Equivalent Circuit Model 1. RE = reference electrode; WE = working electrode; R_s = electrolyte solution resistance; C_c = capacitance associated with the coating; R_c = resistance associated with the coating; C_{dl} = double layer capacitance; R_{ct} = charge transfer resistance.

elements associated with the coating/steel interface. A resistance and capacitance for the surface states of the steel and for the side of the coating in contact with the steel. The surface state of the steel is considered to include the natural occurring oxides and plasma polymer, if any. There is also a resistance and capacitance associated with the surface state of the organic coating, since the surface properties are generally much different from the bulk characteristics of the material. This parallel contribution is in series with the interfacial elements as is the contribution for the bulk coating properties (Q_c and R_c). A constant phase element (Q) is used in place of a coating capacitance, which more accurately models the non-ideal behavior of the coating due to the complex electrochemical reactions taking place [44].

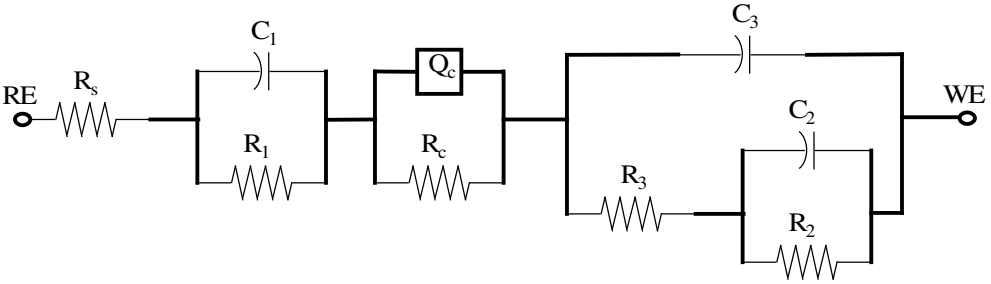

Figure 22. Schematic diagram of Equivalent Circuit Model 2. RE = reference electrode; WE = working electrode; R_s = resistance of electrolyte solution; C_1/R_1 = capacitance and resistance of coating's outer surface state; Q_c = CPE for coating capacitance; R_c = coating resistance; C_2/R_2 = capacitance and resistance of coating's inner surface state; C_3/R_3 = capacitance and resistance of metal surface state (including oxides or oxides + PP).

Since neither of these models represented what was taking place within the studied coating systems, an equivalent circuit model was derived from a combination of the previous two. After investigating many different configurations for the circuit elements, Model 3 shown in Figure 23a was generated. This model design contains two groups of circuit elements. One has the parameters related to the surface state of the organic coating grouped with the resistance and capacitance for the bulk of the coating. The other is the plasma polymer coating parameters coupled with the plasma polymer/metal surface interfacial contributions. This equivalent circuit was used to model the primer/plasma polymer/metal coating systems with and without oxides on the surface. The model had to be modified to represent the control samples because they did not have a plasma polymer deposited onto the surface. For these coating systems (samples A and D) Model 4 shown in Figure 23b was used, where the resistance and capacitance related to the plasma polymer have been removed. Both models generated

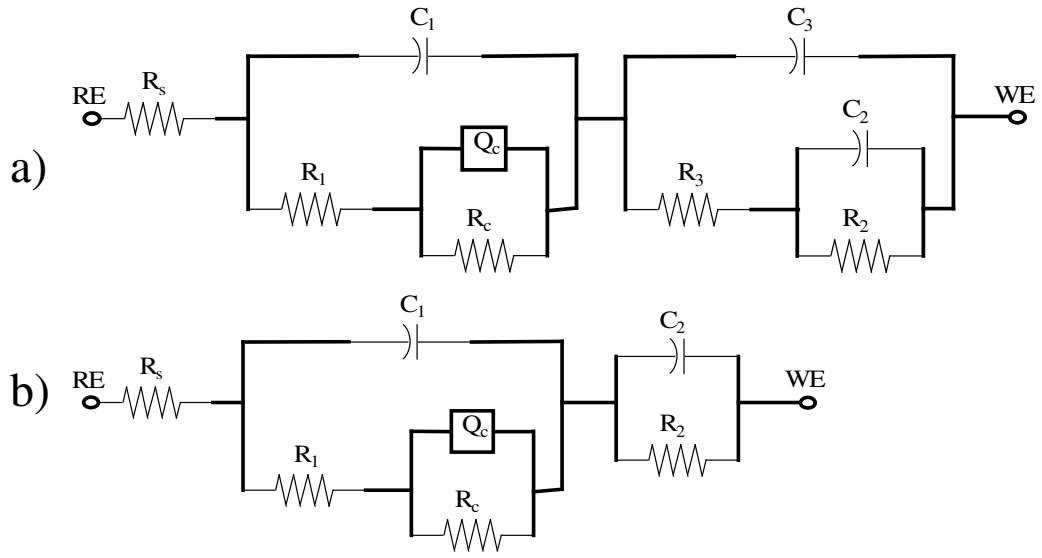

Figure 23. Schematic diagrams for a) Model 3 and b) Model 4. RE = reference electrode; WE = working electrode; R_s = electrolyte solution resistance; C_1/R_1 = capacitance and resistance of the coating surface state; Q_c = CPE for the coating capacitance; R_c = resistance of the coating; C_2/R_2 = double layer capacitance and charge transfer resistance at the PP/metal interface; C_3/R_3 = capacitance and resistance of the plasma polymer film.

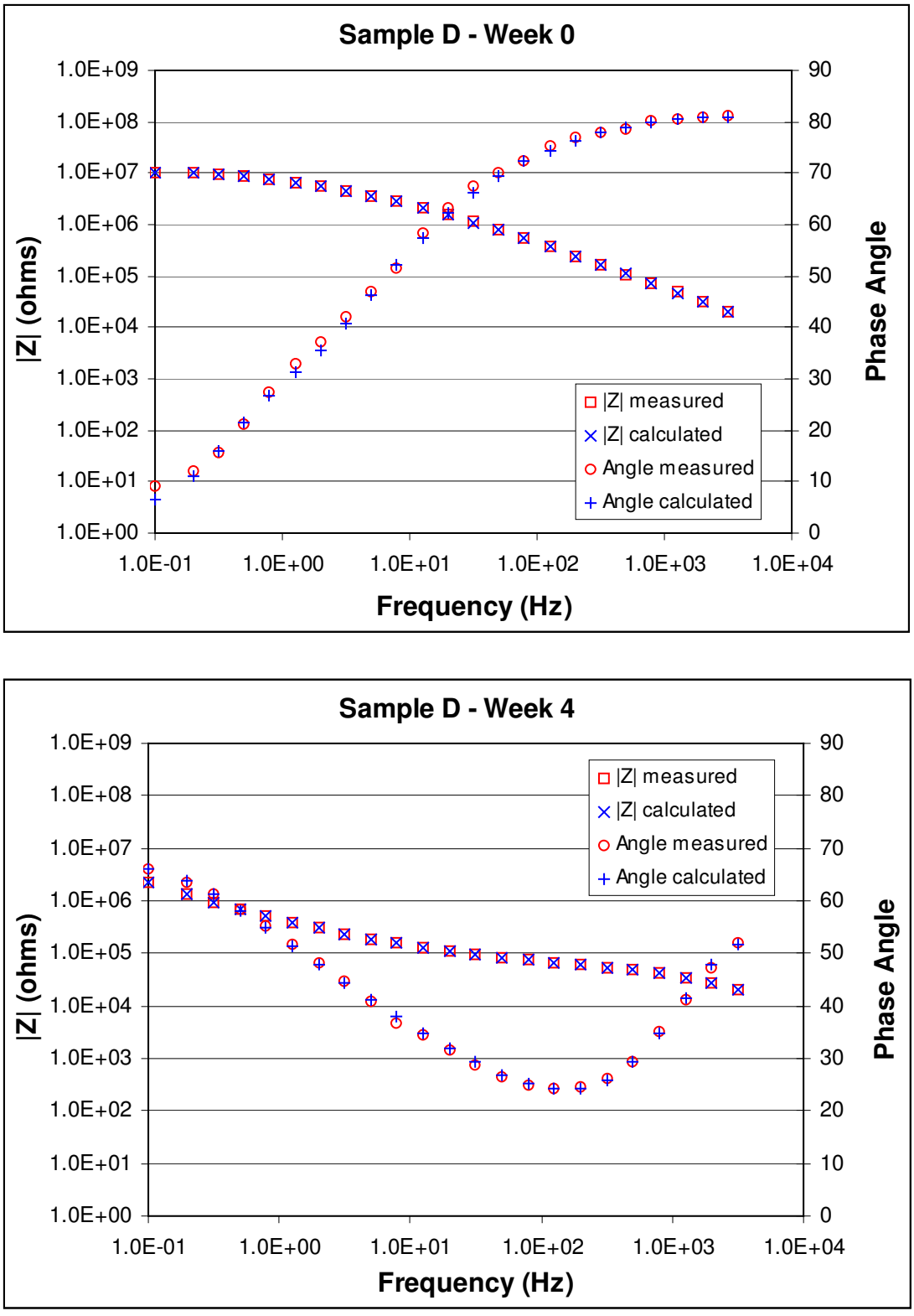

Figure 24. Plots showing the curve fit for the calculated values of the impedance and phase angle during the initial measurement and week 4 measurement.

plots with an excellent fit to the measured impedance and phase angle data (chi squared < 10^{-3}), shown in Figure 24.

Using Models 3 and 4, the electrochemical parameters for all six coating systems were calculated. These values were plotted to correlate a change in parameter values over the period of the GM scab test to the decline in impedance modulus observed in the Bode plots. It was determined that the critical factors are the conditions at the coating/metal interface and performance of the plasma polymer film.

The first noticeable trend looking at Figure 25 is the initial decrease in the charge transfer resistance (R_2) and the increase in double layer capacitance (C_2) at the coating/metal interface for the spray painted samples. This is the expected result as these samples experienced a dramatic drop in impedance modulus within the first week of the scab test. The increase in the capacitance can be attributed to a water/metal interface forming at the substrate surface. This is caused from delamination of the coating, which is expected because of the poor adhesion results from the tape test. The build up of a water layer at the interface provides a means for salt intrusion, which is the reason for the decrease in resistance since the salt intrusion path short circuits the resistive layer. These interfacial parameters, like the low frequency impedance modulus, all converge to the same value by the second week of the corrosion test.

The plasma polymer film, represented by C_3 and R_3, performed differently for samples B and C. Even though the sample with oxides present at the surface (sample B) initially had a higher resistance than the oxide-free sample (sample C), it dropped steadily whereas sample C remained constant. The same is true for the capacitance. Initially slightly lower, sample B increased resulting in better performance for sample C which only increased a little.

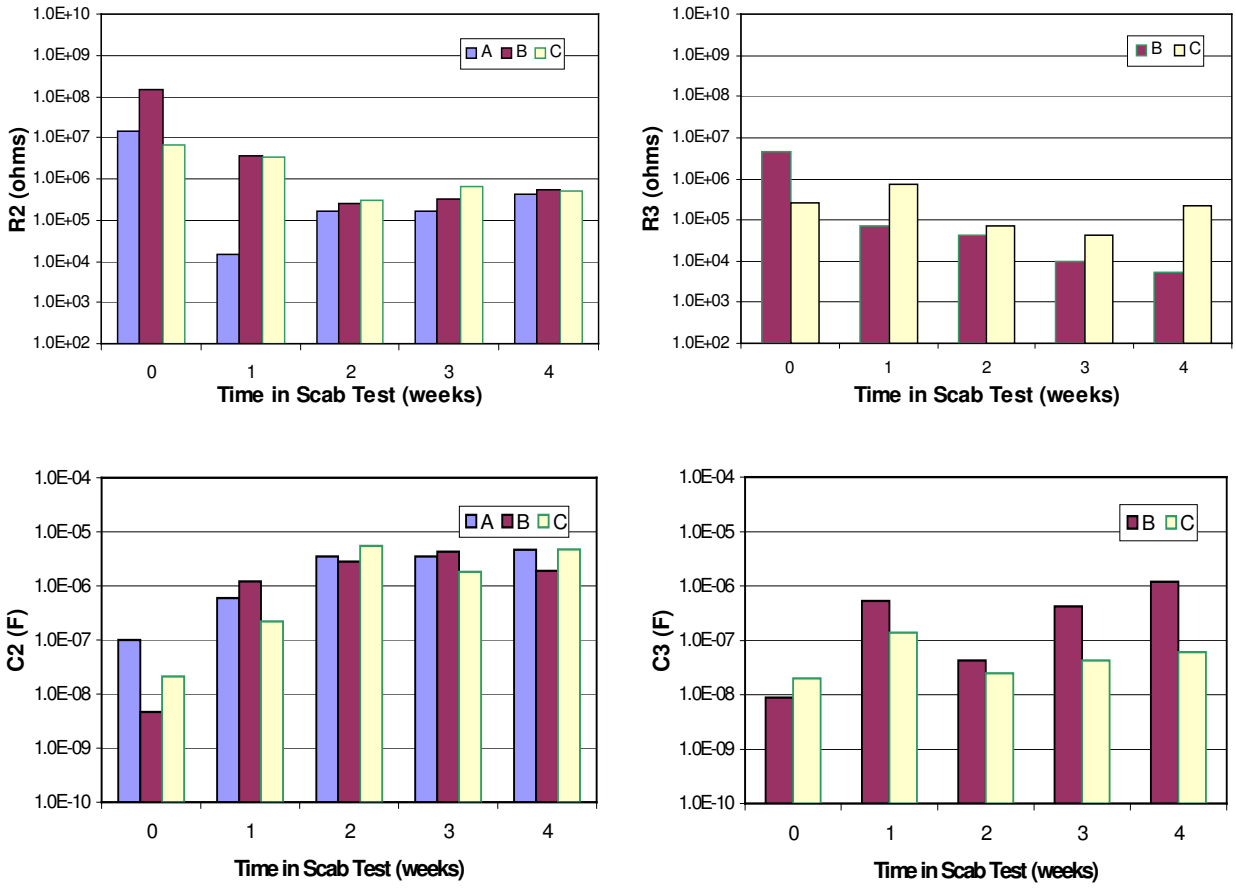

Figure 25. Values of the parameters associated with the interfacial components of samples A, B, and C for each week during corrosion (GM scab) testing.

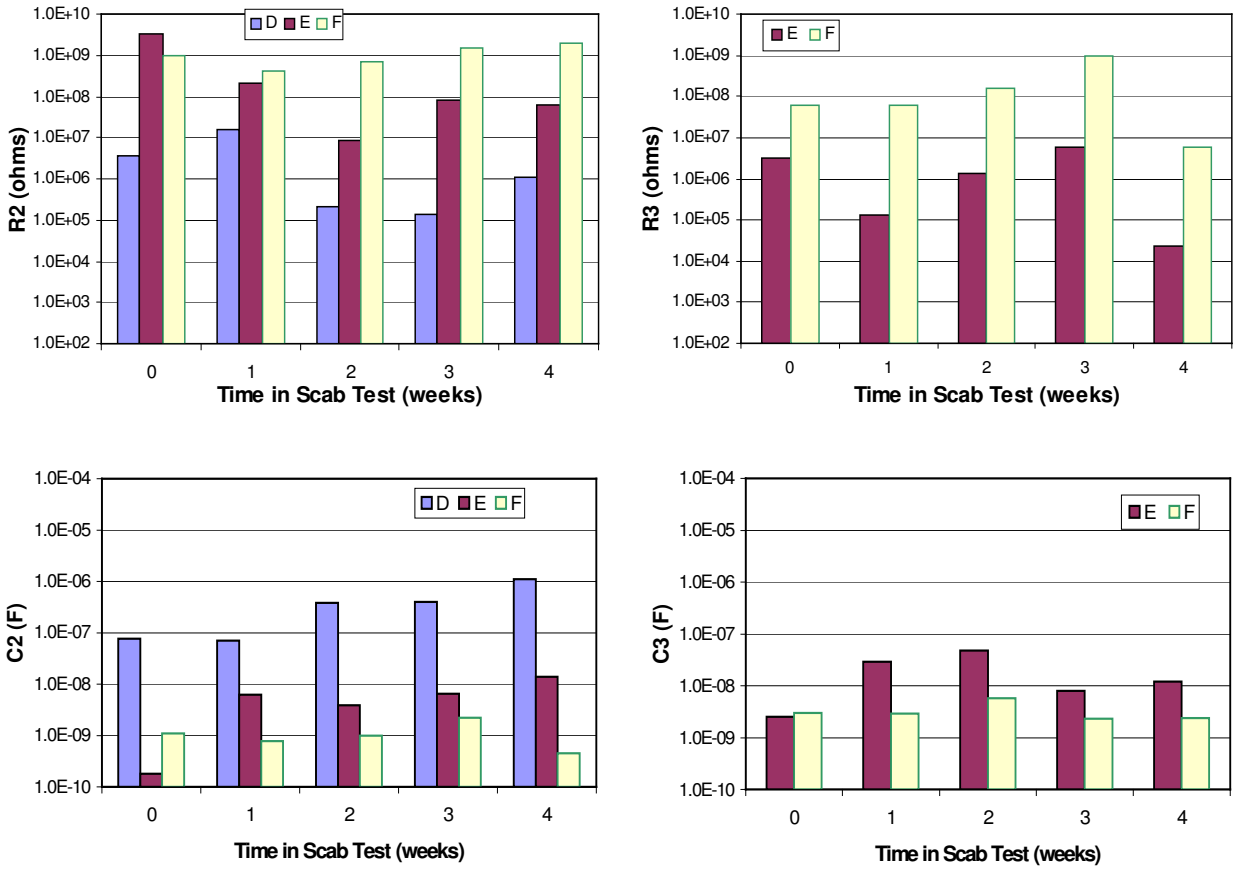

Figure 26. Values of the parameters associated with the interfacial components of samples D, E, and F for each week during corrosion (GM scab) testing.

Figure 26 shows the plots for these same parameters but for the E-coated samples (samples D, E, and F). Again, these results correlate well with the impedance values from the Bode plots. First, looking at the interface where the corrosion takes place, it is evident that the surface preparation contributes significantly to the coating performance. The oxide-free coating (sample F) outperformed all the others with a high charge transfer resistance (R_2 ~ 10^9 ohms) that remained unchanged throughout the corrosion test. Sample E, although initially slightly higher, dropped one order of magnitude indicating a small amount of salt intrusion taking place. The control (sample D) also decreased approximately one order of magnitude from its lower initial resistance value. The double layer capacitance (C_2) increases accordingly for samples D and E and holds at 10^{-9} farads for sample F. These results are consistent with the impedance values reported and the corrosion width results from the previous section.

As expected, the plasma polymer films in the E-coated systems exhibited much better barrier characteristics than the spray painted systems given the higher resistance values and corresponding lower capacitance values. They did have a common trend, however. The oxide-free coating (sample F) outperformed the other coating (sample E) with a capacitance that remained fairly constant and a resistance that only had a small decline in week four of the corrosion test. The capacitance for sample E increased one order of magnitude over the course of the test, and a similar decrease was shown for the resistance.

It was previously shown (Figure 14) that a plasma polymer of TMS deposited onto an oxide-free steel surface produces a much denser and more highly cross-linked film than when oxides are present. When oxides are present on the surface, they are incorporated into the plasma polymer, via the competitive ablation and polymerization

mechanism, creating these weaker boundary properties. This will allow for more water uptake by the film, resulting in the expected capacitance increase over the course of the corrosion test period witnessed in Figures 25 and 26.

The initially lower capacitance (C_3) for samples B and E (primer/PP/oxides/substrate) is likely due to the significant amount of oxygen contained within the plasma polymer layer. The capacitance is directly related to the dielectric strength of the material. The Si concentration in the film is lowered by the presence of oxygen which reduces the effective dielectric strength of the film (dielectric constant of Si = 11.0 and O_2 = 1.0). This becomes insignificant once water is absorbed by the film because water is a much stronger dielectric material (dielectric constant of H_2O = 88). The capacitance will increase according to the amount of water uptake by the film.

One of the key points of this study is that each coating layer contributes to the overall coating performance and should not be chosen solely on its individual corrosion resistance. This is evident with the performance difference between two identical sets of plasma polymer films with different primer coatings. As mentioned, there was less water uptake by the plasma polymer films that were E-coated (samples E and F) and exhibited good adhesion. With poor adhesion, the plasma polymer film is susceptible to more water due to pool formation at the interface. More water will consequently be absorbed resulting in the higher capacitance values seen for the spray painted samples (samples B and C).

Another example of a coating component performing better in one system than in another is with the organic coating. Figure 27 shows the results from the equivalent circuits for the constant phase element (CPE) for the capacitance of the organic coating. It is evident that the underlying layer is crucial to the performance of the coating. The

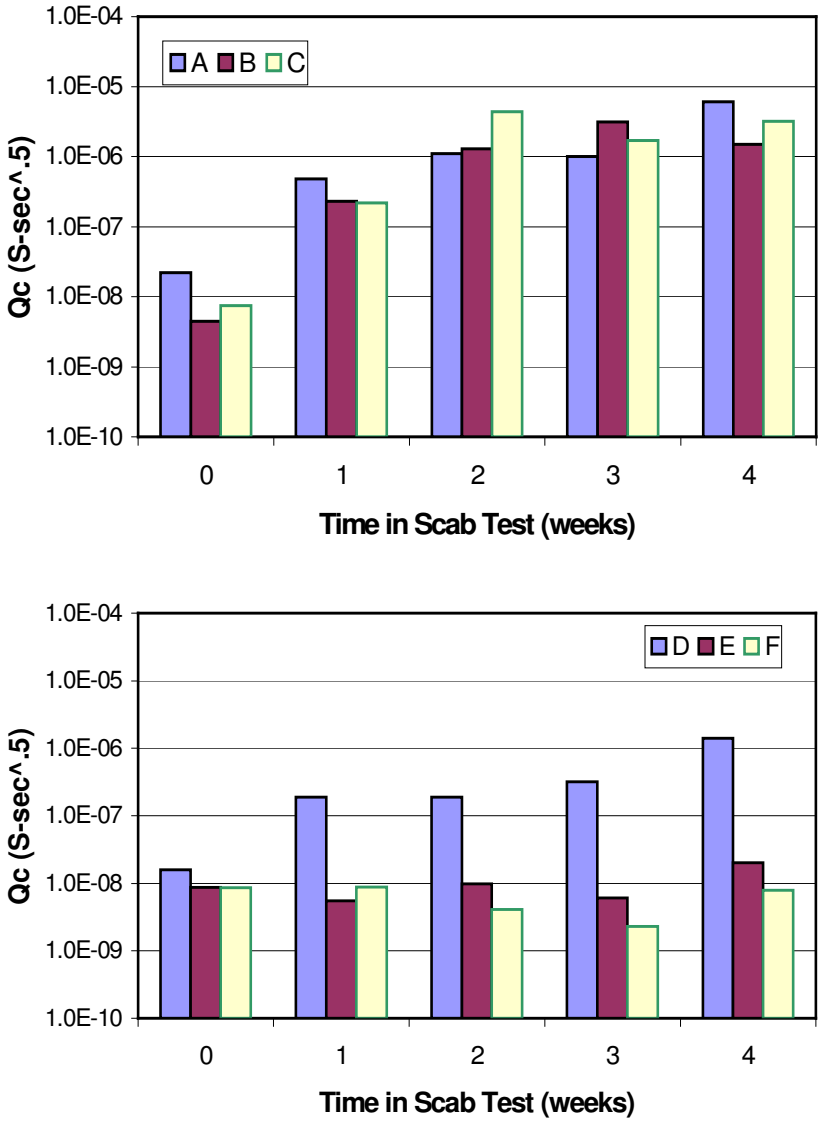

Figure 27. Values of the CPE for samples A, B, and C and samples D, E, and F for each week during corrosion (GM scab) testing.

deposition of the adhesion enhancing TMS plasma polymer provides a suitable layer for application of the E-coat. Without it (sample D), the E-coat's performance is unsatisfactory, behaving similar to the spray painted samples. The poor barrier properties of the spray painted primer are obvious from this plot. The CPE drop indicates severe water uptake by the coating for all three samples after one week of the corrosion test.

Figure 28 compares the initial and final values of the key parameters contributing to the performance of the coating system after being subjected to the corrosion (GM scab) test. This is simplifying Figures 25 and 26 in order to compare the different interface engineered coating systems and the affect a corrosive environment has on each. These plots clearly show the dramatic difference between the samples with bad adhesion (samples A, B, C, and D) and those with good adhesion (samples E and F). Even though sample D was prepared with the E-coat, without the TMS plasma polymer layer it does not achieve good adhesion and therefore behaves like the spray painted samples. After four weeks these four samples had a much lower resistance (R_2) and higher capacitance (C_2) at the coating/metal interface signifying electrolyte solution in contact with the base metal which initiates corrosion. There is less electrolyte penetration when good adhesion is accomplished.

The resistance is much higher, and a lower capacitance, for samples E and F. Sample E still has a drop in resistance and a corresponding increase in capacitance over the test period. Sample F with the coating system E-coat/TMS/oxide-free steel is the only one to have final parameter values unchanged from the beginning of the corrosion test. Looking at R_3 and C_3 it can be stated that the oxide-free plasma polymer film (samples C and F) outperforms the oxide containing film (samples B and E) whether there is good adhesion or not. The performance is enhanced, however, with good

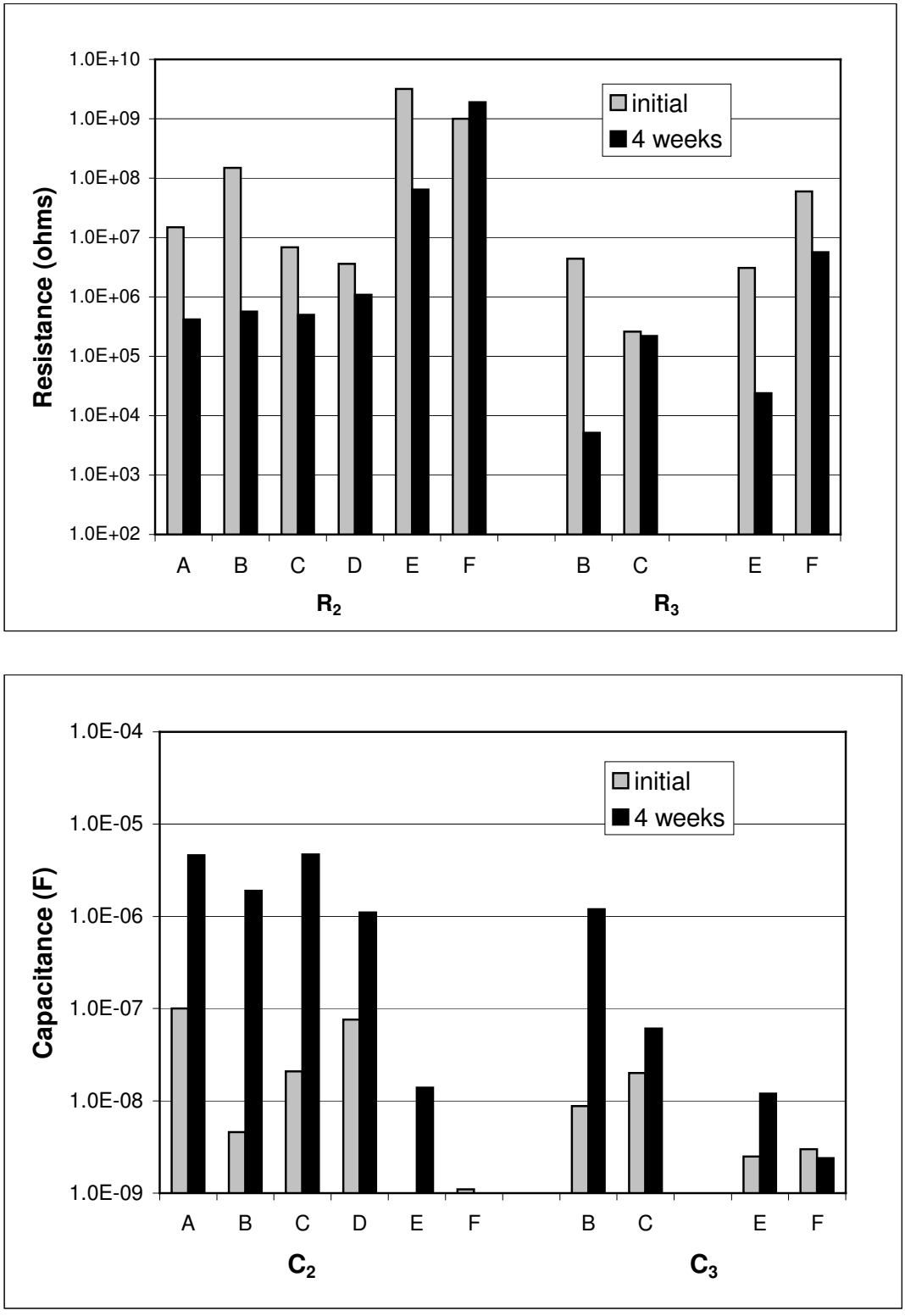

Figure 28. Changes in the resistance (R_2 and R_3) and capacitance (C_2 and C_3) from the initial value to the final value after the four week corrosion (GM scab) test for all six samples.

adhesion. Reviewing the final values of these coating parameters it is clear that the overall coating performance decreases in the following sample order:

$$F >> E >> D > C \sim B \sim A$$

These results are supported by the corrosion width and tape test measurements reported earlier. Good adhesion is vital to the corrosion protection potential of a coating system. This has been achieved by creating an oxide-free steel surface followed by deposition of a TMS plasma polymer film. The two equivalent circuit models proposed in this study (Figure 23) have accurately simulated the EIS data to generate expected parameter values relating to the actual conditions of the coating.

5. CONCLUSIONS

The treatment of CRS prior to applying a primer is a critical factor in the overall coating performance. The interface engineered systems of TMS deposited onto an oxide-free surface, produced by the cathodic (argon + hydrogen) treatment, outperformed similar coatings that contained the native oxide layer. A TMS layer with a refractive index near 2.0 was obtained with optimal conditions of the (argon + hydrogen) pretreatment, resulting in the best performance of the TMS/(oxide-free) steel system. Excellent dry and wet adhesion was observed for this coating, as well as the smallest corrosion width determined by corrosion propagation from a damaged site.

EIS generated expected results based on the linear polarization values of the plasma treated samples. The E-coat/TMS/(oxide-free) steel system was the best coating, having no drop in impedance modulus at the low frequency for the entire four week corrosion (GM scab) testing period.

The two equivalent circuits, proposed in this study, modeled the EIS experiments with a good visual fit and low chi squared values ($< 10^{-3}$). More importantly, however, the circuit elements calculated from the simulated data represented the actual performance of the coating system, supporting the ability of these equivalent circuits to model the coating systems presented in this study.

From this data, critical factors for the performance were able to be determined. The low CPE values for the spray painted samples reflects the poor barrier properties of this primer. These samples also exhibited poor adhesion resulting in water pool formation at the primer/substrate interface and subsequent delaminating of the primer reflected in the interfacial capacitance increase. A corresponding decrease in resistance

relates to the initiation of corrosion caused by the electrolyte/metal contact. All of these samples showed significant degradation of coating parameters after one week of the corrosion test and converged to similar values of poor performance.

The E-coated systems performed significantly better as expected because of the good adhesion. The equivalent circuits calculated much lower values of the interfacial capacitance and higher values of the resistance relating to a larger area of coating attached to the substrate and correspondingly less corrosion. A small increase in this capacitance indicated some pool formation was present with the oxygen containing coatings, but the E-coat on the oxide-free sample showed no signs of delaminating. Contributing to the good performance is the use of a less permeable coating. The E-coat allows fewer water molecules to diffuse to the interface, and in conjunction with the water insensitive adhesion, less pool formation is observed.

With the use of the two proposed equivalent circuits, it appears that a more detailed analysis of the corrosion resistance of a coating system can be achieved. Results obtained from these models correlated well with the data from other accepted corrosion tests. Testing these models with a wider range of samples is essential to confirm their accuracy.

REFERENCES

1. K.D. Connors, W.J. van Ooij, D.J. Mills, and G.P. Bierwagen, *British Corrosion Journal*, **35**(2), 141-144 (2000).

2. W.J. van Ooij, D.Q. Zhu, G. Prasad, S. Jayaseelan, Y. Fu, and N. Teredesai, *Surface Engineering*, **16**(5), 386-396 (2000).

3. V. Subramanian and W.J. van Ooij, *Surface Engineering*, **15**(2), 168-172 (1999).

4. G.P. Sundararajan and W.J. van Ooij, *Surface Engineering*, **16**(4), 315-320 (2000).

5. L. Domingues, C. Oliveira, J.C.S. Fernandes, and M.G.S. Ferreira, *Electrochimica Acta*, **47**, 2253-2258 (2002).

6. "Basics of Electrochemical Impedance Spectroscopy", Application Note AC-1, EG&G Princeton Applied Research.

7. http://www.gamry.com/App_Notes/EIS_Modeling/EIS_Modeling.htm.

8. M. Chen, Q.S. Yu, C.M. Reddy, and H.K. Yasuda, *Corrosion*, **56**(7), 709-721 (2000).

9. H.H. Uhlig, "Iron and Steel" in The Corrosion Handbook, H.H. Uhlig, ed., John Wiley & Sons, New York, NY, p. 125, 1948.

10. M.B. Knaster and J.M. Parks, *Corrosion: Coatings and Steels*, **649**, 23-32 (1986).

11. Z.W. Wicks, Jr., "Corrosion Protection by Coatings", Federation of Societies for Coatings Technology, Philadelphia, PA, 1987.

12. M.G. Fontana and N.D. Greene, "Electrochemical Aspects" in Corrosion Engineering, McGraw-Hill, Inc., New York, NY, p. 10, 1967.

13. V.M. Darsy, "Phosphate Coatings" in The Corrosion Handbook, H.H. Uhlig, ed., John Wiley & Sons, New York, NY, p. 867, 1948.

14. D.B. Freeman, "Phosphating and Metal Pre-treatment: A Guide to Modern Processes and Practice", Industrial Press, New York, NY, 1986.

15. A. Sabata, W.J. van Ooij, and R.J. Koch, *Journal of Adhesion Science and Technology*, **7**(11), 1153-1170 (1993).

16. B.H. Chun, Ph.D. Dissertation, University of Missouri-Columbia, 1994.

17. W.J. van Ooij, A. Sabata, D.B. Zeik, C.E. Taylor, F.J. Boerio, and S.J. Clarson, *Journal of Testing and Evaluation*, **23**(1), 33-40 (1995).

18. H.K. Yasuda, B.H. Chun, D.L. Cho, T.J. Lin, D.J. Yang, and J.A. Antonelli, *Corrosion*, **52**(3), 169-176 (1996).

19. H.K. Yasuda, "Plasma Polymerization", Academic Press, Inc., Orlando, FL, 1985.

20. http://www.eurobonding.org/English/Oberflaechen/Plasma_polymerization.htm.

21. Y. Lin and H.K. Yasuda, *Journal of Applied Polymer Science*, **60**, 543 (1996).

22. H.K. Yasuda and Q.S. Yu, *Journal of Vacuum Science and Technology*, **A19**(3), 773-781 (2001).

23. S. Gaur and G. Vergason, "Plasma Polymerization: Theory and Practice", *Society of Vacuum Coaters*, 267-271 (2000).

24. C.M. Reddy, "Improved Corrosion Protection of Aluminum Alloys by Low Temperature Plasma Interface Engineering", Ph.D. Dissertation, University of Missouri-Columbia, 1998.

25. J.G. Zhao and H.K. Yasuda, "The Effect of Magnetic Field Configuration in the Cathodic Polymerization Systems with Two Anode Magnetrons", DARPA Grant AF F33615-96-C-5055 Final Report, 237-245 (2001).

26. N. Morosoff, "An Introduction to Plasma Polymerization" in Plasma Deposition, Treatment and Etching of Polymers, d'Agostino, R. ed., Academic Press, San Diego, CA (1990).

27. H.K. Yasuda, T. Hsu, E.S. Brandt, and C.N. Reilley, *Journal of Polymer Science: Polymer Chemistry Edition*, **16**(2), 415-425 (1978).

28. S. Lucas, P. Vanden Brande, and A. Weymeersch, *Surface and Coatings Technology*, **100-101**, 251-259 (1998).

29. H.P. Schreiber, Y.B. Tewari, and M.R. Wertheimer, *Ind. Eng. Chem. Prod. Res. Dev.*, **17**(1), 27 (1978).

30. T.F. Wang, "Corrosion Protection of Automotive Steel by Plasma Polymer-Electrocoating Combined Coating System", Ph.D. Dissertation, University of Missouri-Columbia, 1994.

31. W.J. van Ooij, D. Surman, and H.K. Yasuda, *Progress in Organic Coatings*, **25**(4), 319-337 (1995).

32. T.F. Wang, T.J. Lin, D.J. Yang, J.A. Antonelli, and H.K. Yasuda, *Progress in Organic Coatings*, **28**(4), 291-297 (1996).

33. H.K. Yasuda, T.F. Wang, D.L. Cho, T.J. Lin, and J.A. Antonelli, *Progress in Organic Coatings*, **30**(1), 31-38 (1997).

34. A. Sabata, W.J. van Ooij, and H.K. Yasuda, *Surface and Interface Analysis*, **20**, 845-859 (1993).

35. http://www.gamry.com/App_Notes/EIS_Primer/EIS_Primer.htm

36. A. Zeng, E. Liu, S. Zhang, S.N. Tan, P. Hing, I.F. Annergren, and J. Gao, *Thin Solid Films*, **426**, 258-264 (2003).

37. O. Baradel and R. Nuttall, Colloquim (Institution of Electrical Engineers), 71, 8/1-8/10 (1994).

38. Y.J. Yu, J.G. Kim, and J.H. Boo, *Journal of Materials Science Letters*, **21**, 951-953 (2002).

39. C. Vautrin-Ul, C. Boisse-Laporte, A. Chausse, P. Leprince, and R. Messina, Iron Corrosion Protection by Plasma-Polymerized Coatings, *Journal of Corrosion Science and Engineering*, **2**, Paper 3, Cambridge, 1999.

40. K.D. Conners, W.J. van Ooij, S.J. Clarson, and A. Sabata, *Journal of Applied Polymer Science: Applied Polymer Symposium*, **54**, 167-184 (1994).

41. G. Grundmeier and M. Stratmann, *Applied Surface Science*, **141**, 43-56 (1999).

42. M.G. Fontana and N.D. Greene, "Corrosion-Rate Measurements" in Corrosion Engineering, McGraw-Hill, Inc., New York, NY, p. 342, 1967.

43. F.P. Ijsseling, *British Corrosion Journal*, **21**(2), 95-101 (1986).

44. http://www.consultrsr.com/resources/eis/cpe1.htm